8-5-2020 1:00 PM

Boosting cellular NAD+ concentration with nicotinamide mononucleotide prevents Doxorubicin-induced cardiotoxicity

Rebecca Dang, *The University of Western Ontario*

Supervisor: Peng, Tianqing, *The University of Western Ontario*

A thesis submitted in partial fulfillment of the requirements for the Master of Science degree in Pathology and Laboratory Medicine

Abstract

Doxorubicin (DOX) is a powerful chemotherapy that functions by interfering with cancer cells' growth. However, the use of DOX is limited due to its detrimental side effects that can lead to serious cardiovascular complications. Our goal is to determine if nicotinamide mononucleotide (NMN) and histone acetyltransferase (HAT) inhibitors can protect against DOX-induced cardiotoxicity. Our findings revealed that DOX reduced NAD^+ concentration and induced damage to H9c2 cells as evidenced by higher caspase-3 activity and lactate dehydrogenase release. Pre-incubation with NMN increased NAD^+ concentration and attenuated DOX-induced damage. There was higher cell viability in the NMN pre-incubated group compared to the vehicle treated group in response to DOX. Furthermore, mice pre-treated with NMN had higher ejection fraction and fraction shortening percentage compared to the vehicle treated group. In contrast, pre-incubation with HAT inhibitors failed to protect DOX-treated cells. Thus, our study suggests that NMN may be a potential drug that prevents DOX-induced cardiotoxicity.

Keywords

cardiotoxicity, cell death, Doxorubicin, histone acetyltransferase, nicotinamide adenine dinucleotide, nicotinamide mononucleotide

Summary for Lay Audience

With about 9.8 million patients worldwide needing treatment annually, chemotherapy is a widely used treatment option for cancer patients. Doxorubicin (DOX) is a well-established chemotherapy drug that is prescribed for a diverse range of cancer types. DOX has a drawback as it causes heart damage, which is referred to as DOX-induced cardiotoxicity. In severe cases, DOX-induced cardiotoxicity can result in heart failure leading to death, even years after the patient has stopped their treatment.

The imbalance between histone deacetylase and histone acetyltransferase activity may be the main cause of DOX-induced cardiotoxicity. Histone deacetylases are enzymes that function to removes chemical molecules called acetyl groups. Previous research in our laboratory showed that nicotinamide riboside, a compound similar to Vitamin B3, protected against DOX-induced cardiotoxicity. We found that when cells take in nicotinamide riboside, it is converted into a molecule called nicotinamide adenine dinucleotide (NAD^+). NAD^+ will activate a group of histone deacetylase called Sirtuins to remove acetyl groups. We predict that histone acetyltransferase, which are enzymes that function to add acetyl groups are involved as well. The exact molecular mechanisms and histone acetyltransferases' involvement in the development of DOX-induced cardiotoxicity are still not completely understood.

The goal of my research is to determine whether there are alternative compounds that can prevent DOX-induced cardiotoxicity. In the first part of my research, I determined if Nicotinamide mononucleotide (NMN) can protect against DOX using a heart cell line and mouse models. NMN is another molecule that converts into NAD^+ to activate histone deacetylase. The second part of my project tests different histone acetyltransferase inhibitors to examine whether they can protect a heart cell line from DOX. The histone acetyltransferase inhibitor functions to block specific histone acetyltransferase members from activating.

The findings from the first part of my research show that NMN increased NAD^+ and functions as a source of cardioprotection against DOX. The second portion of my study shows that specific histone acetyltransferase family members are not involved in DOX-

induced cardiotoxicity. Hence, my research contributes to advancing current scientific knowledge in the field of DOX-induced cardiotoxicity and discovering preventive therapeutics options for millions of cancer patients.

Dedication

In memory of John Smith
(1936-2018)

"For I was hungry and you gave me food, I was thirsty and you gave me drink, I was a stranger and you welcomed me."
Matthew 25:35

Acknowledgments

I want to express my gratitude to my supervisor, Dr. Tianqing Peng for letting me be a part of the Peng Lab. I appreciated all of your efforts and time for helping me through graduate school. Thank you to my advisory committee members, Dr. Douglas Jones and Dr. Martin Duennwald for always providing me with provoking insights and constructive feedback. Special thanks to the members of the Peng Lab including Dr. Rui Ni, Ting Cao, Xiaoyun Ji, Nima Nalin, Liwen Liang, and Mengxiao Zhang for guiding me through my experiments.

To the Arriola family, thank you for being with me from the moment I started graduate school until the end of my graduate journey. A special thank you to Cynthia for always being one phone call away. Your endless support and willingness to listen to my stories motivated me through the difficult times of graduate school.

Finally, and most importantly to my mom, dad, and brother. I would not be where I am today without your unconditional love and support. Thank you for everything.

Table of Contents

Abstract ii

Summary for Lay Audience iii

Dedication v

Acknowledgments vi

Table of Contents vii

List of Tables xi

List of Figures xii

List of Abbreviations xiv

Chapter 1 1

1 Introduction 1

1.1 Doxorubicin 1

1.1.1 DOX's mechanisms of action 2

1.1.2 DOX-induced cardiotoxicity 2

1.1.3 Treatment Options for DOX-induced cardiotoxicity 3

1.1.4 DOX-induced cardiotoxicity's mechanism of action 3

1.2 Nicotinamide adenine dinucleotide 4

1.2.1 Salvage NAD^+ Pathway 6

1.2.2 Nicotinamide Riboside 7

1.2.3 Nicotinamide Mononucleotide 8

1.3 Histone Deacetylase Family 9

1.3.1 SIRT1 and DOX-induced cardiotoxicity 10

1.3.2 SIRT3 and DOX-induced cardiotoxicity 10

1.4 Histone Acetyltransferase Family 10

1.4.1 GCN5 and Butyrolactone 3 inhibitor 11

1.4.2 TIP60 and MG149 inhibitor 12

1.4.3 p300/CBP, C646, and HAT inhibitor II 13

1.5 Proposed Model 16

1.6 Hypothesis 17

1.7 Specific Aims 17

1.7.1 To evaluate the utility of H9c2 cell culture as an *in vitro* model to study DOX-induced cardiotoxicity 17

1.7.2 To determine if NMN protects against DOX-induced cardiotoxicity through boosting cellular NAD^+ concentration in H9c2 cells and adult mice hearts 17

1.7.3 To examine the effect of pharmacological HAT inhibitors on DOX-induced cardiotoxicity 17

Chapter 2 19

2 Material and Methods 19

2.1 Cell Culture 19

2.2 Caspase-3 Activity Measurement 20

2.3 Lactate Dehydrogenase Release Assay from Clontech 21

2.4 NAD^+ Microplate Reader Assay from Cohesion Biosciences 21

2.5 Caclein AM Cell Viability Assay from Trevigen 22

2.6 Animals 22

2.7 Echocardiography 22

2.8 Evans Blue Staining 23

2.9 Solution preparation 24

2.9.1 DOX 24

2.9.2 NMN 24

2.9.3 NAD^+ free acid 25

2.9.4 Butyrolactone 3 25

2.9.5 MG149 25

2.9.6 C646 25
2.9.7 HAT inhibitor II 26
2.10 Data Analysis 26
Chapter 3 28
3 Results 28
3.1 DOX increases LDH release in a dose-dependent manner 28
3.2 DOX increases caspase-3 activity in a dose-dependent manner 29
3.3 DOX reduces H9c2 cells viability in a dose-dependent manner 30
3.4 DOX treatment results in lower NAD^+ concentration in H9c2 cells 32
3.5 NMN treatment results in higher NAD^+ concentration in H9c2 cells 33
3.6 NMN abrogates LDH release in H9c2 cells 34
3.7 NMN abrogates caspase-3 activity in H9c2 cells 35
3.8 NMN abrogates DOX-induced loss of H9c2 cell viability 36
3.9 NAD^+ free acid abrogates DOX-induced death in H9c2 cells 37
3.10 NAD^+ free acid decreases caspase-3 activity in H9c2 cells treated with DOX 38
3.11 Administration of NMN improves myocardial function in DOX-injected mice 39
3.12 NMN reduces cardiac injury in DOX injected mice 43
3.13 Inhibition of HAT GCN5 with Butyrolactone 3 does not protect H9c2 cell viability against DOX-induced cardiotoxicity 46
3.14 Inhibition of HAT TIP60 with MG149 does not block the effect of DOX treatment on H9c2 cell viability 47
3.15 Inhibition of HAT p300/CBP with C646 does not block DOX's effect on H9c2 cell viability 48
3.16 Inhibition of HAT p300 with HAT inhibitor II does not block DOX effect on H9c2 cell viability 49
Chapter 4 50
4 Discussion, Limitations, and Future Directions 50
4.1 Discussion 50

4.1.1 DOX induces damage in a dose-dependent manner 50
4.1.2 Increasing NAD^+ concentration prevents DOX damage in H9c2 cells 50
4.1.3 NMN protects mice hearts against DOX 51
4.1.4 Selective HAT inhibitors have no effect on H9c2 cells treated with DOX 52
4.2 Limitations 54
4.3 Future Directions 55
4.4 Project Significance 56
4.5 Concluding Remarks 56
References 57
Curriculum Vitae 67

List of Tables

Table 1: Summary of the chemical structure, formula, and function of key biological and chemical molecules. 15

Table 2: Components in 1L of D-Hanks' solution..... 20

Table 3: Components in 100 mL of Caspase-3 Lysis Buffer..... 21

Table 4: Components in 100 mL of Caspase-3 Assay Buffer. 21

Table 5: Components in 1L of 1X PBS. 24

Table 6: List and descriptions of reagents. 26

Table 7: Echocardiography analysis on adult C57BL/6 male mice injected with either NMN (500 mg/kg) or saline for 30 minutes, then a DOX (20 mg/kg) or saline injection. 39

List of Figures

Figure 1: Chemical Structure of Daunorubicin and DOX. 2

Figure 2: Chemical structure of NAD^+. 5

Figure 3: The salvage pathway to synthesizing NAD^+. 7

Figure 4: Chemical structure of NR. 8

Figure 5: Chemical structure of NMN. 9

Figure 6: Chemical structure of Butyrolactone 3. 12

Figure 7: Chemical structure of MG149. 13

Figure 8: Chemical structure of HAT inhibitor II. 14

Figure 9: Chemical structure of C646. 14

Figure 10: Diagram of the HAT family members and inhibitors used in this study. 15

Figure 11: Proposed Model of DOX-induced cardiotoxicity. 16

Figure 12: Effect of DOX on LDH release in H9c2 cells. 28

Figure 13: Effect of DOX on caspase-3 activity in H9c2 cells. 29

Figure 14: Effect of DOX on H9c2 cells viability. 31

Figure 15: NAD^+ concentration after treatment with DOX in H9c2 cells. 32

Figure 16: NAD^+ concentration after treatment with NMN in H9c2 cells. 33

Figure 17: Effect of NMN on LDH release in H9c2 cells. 34

Figure 18: Effect of NMN on caspase-3 activity in H9c2 cells. 35

Figure 19: Effect of NMN on DOX-induced loss of H9c2 cell viability 36

Figure 20: Effect of NAD^+ free acid on DOX-induced cell death in H9c2 cells..... 37

Figure 21: Effect of NAD^+ free acid on caspase-3 activity in H9c2 cells treated with DOX. 38

Figure 22: Representative echocardiography image of adult mice in the acute DOX-induced cardiotoxicity study..... 40

Figure 23: Effect of NMN on ejection fraction in DOX-injected mice..... 41

Figure 24: Effect of NMN on fractional shortening in DOX-injected mice..... 42

Figure 25: Representative micropictures of Evans Blue staining and nuclear staining..... 44

Figure 26: Quantification of Evans Blue positive cells in DOX injected mice..... 45

Figure 27: Effect of Butyrolactone 3 on H9c2 cell viability. 46

Figure 28: Effect of MG149 on H9c2 cell viability..... 47

Figure 29: Effect of C646 on H9c2 cell viability. 48

Figure 30: Effect of HAT inhibitor II on H9c2 cell viability. 49

List of Abbreviations

ACE	Angiotensin converting enzyme
ATP	Adenosine triphosphate
BW	Body weight
CBP	CREB-binding protein
DMEM	Dulbecco's Modified Eagle Medium
DMSO	dimethyl sulfoxide
DOX	Doxorubicin
EF	Ejection fraction
ELP3	Elongator protein 3
ENT	Equilibrative nucleoside transport
FBS	Fetal bovine serum
FS	Fractional shortening
GCN5	General Control Non-depressible 5
GNAT	Gcn5-related N-acetyltransferase
HAT	Histone acetyltransferase
HDAC	Histone deacetylase
HR	Heart rate
HW	Heart weight
LDH	Lactate dehydrogenase
LV	Left ventricle
LVAWd	Left ventricular anterior wall at diastole
LVAWs	Left ventricular anterior wall at systole
LVIDd	Left ventricular internal diameter at diastole
LVIDs	Left ventricular internal diameter at systole
LVPWd	Left ventricular posterior wall at diastole
LVPWs	Left ventricular posterior wall at systole
MYST	**M**OZ, **Y**BF2/SAS3, **S**AS2, **T**IP60
NAD^+	Nicotinamide adenine dinucleotide
NAM	Nicotinamide
NAMPT	Nicotinamide phosphoribosyltransferase
NAPRT	Nicotinate phosphoribosyltransferase
NCOA3/ACTR	Nuclear receptor Coactivator 3
NMN	Nicotinamide mononucleotide
NMNATs	Nicotinamide mononucleotide adenylyl transferases
NR	Nicotinamide riboside
NRCF	Nuclear receptor cofactors
NRK	Nicotinamide riboside kinases
P/S	Penicillin-streptomycin
PARP	Poly (ADP-ribose) polymerase
PCAF	p300/CBP-associated factor
ROS	Reactive Oxygen Species
SIRT	Sirtuin
SIRT1	Silent mating type information regulation 2 homolog 1

SIRT3	Silent mating type information regulation 2 homolog 3
Slc12a8	Solute carrier family 12 member 8
SRA	Steroid Receptor Coactivator
TAF1	TATA-box binding protein associated factor 1
TIP60	Tat-interactive protein 60 KDa
TSA	Trichostatin A

Chapter 1

1 Introduction

Cancer is one of the leading causes of death worldwide. According to the World Health Organization, there will 10-11 million new cancer cases diagnosed annually by 2030 (1). Chemotherapy is a widely used treatment option for patients at different cancer stages to prevent cancer cell proliferation. Anthracyclines are a class of drugs that include Doxorubicin and are one of the most effective types of chemotherapy (2).

1.1 Doxorubicin

Doxorubicin (DOX), under the brand name Adriamycin, is a first line chemotherapeutic given to children and adults with various cancer types such as breast cancer or leukemias (3). DOX was discovered in the 1960's by Italian researchers isolating anti-cancer compounds produced by soil microbes (4). Researchers found that colonies of *Streptomyces peucetius* produced red pigments with antibiotic properties and named the compound Daunomycin (4). After discovering that a French research group isolated the same compound, the compound became known as Daunorubicin. Daunorubicin eventually was renamed DOX after a modification in the hydroxyl group on carbon 14 (4). The chemical structure of DOX contains an aglyconic moiety (tetracyclic ring with quinine-hydroquinone adjacent groups, methoxy side chain, and carbonyl group) and sugar component (also known as Daunosamine) (Figure 1) (5).

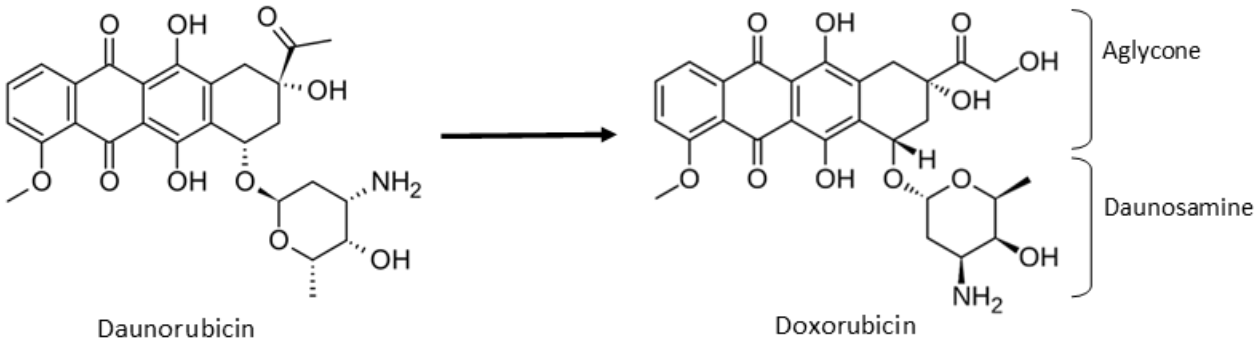

Figure 1: Chemical Structure of Daunorubicin and DOX.

Daunorubicin and DOX structure differs in a hydroxyl group. The chemical formula of DOX is $C_{27}H_{29}NO_{11}$ and the molecular weight is 543.56 g/mol. The chemical formula of Daunorubicin is $C_{27}H_{29}NO_{10}$ and the molecular weight is 527.52 g/mol. Figure created using images from WikiMedia Commons (6,7).

1.1.1 DOX's mechanisms of action

As a member of the class I Anthracycline family, DOX is administered intravenously and rapidly taken up by cells with an initial half-life of about 5 minutes (5,8). The terminal half-life of DOX is between 20-48 hours from the tissue (8). DOX functions to initiate cancer cell growth arrest through various mechanisms. One mechanism is through intercalation between base pairs of double-stranded DNA to prevent DNA topoisomerase II activity, which is required for DNA replication, transcription, and recombination (9). DOX intercalates between the base pair of the DNA, resulting in disruption of DNA topoisomerase II activity. Therefore, DNA replication is stopped, and cancer cells cannot proliferate. Another mechanism is excessive reactive oxygen species (ROS) produced in cells. DOX is oxidized from a quinone to semiquinone, an unstable metabolite to produce free radicals following cellular uptake (10). The release of ROS leads to DNA damage, oxidative stress, and cell death by apoptosis in cancer cells (11).

1.1.2 DOX-induced cardiotoxicity

The major problem with DOX is its detrimental side effects on the heart, leading to serious cardiovascular complications such as heart failure and hypertension (12). Some factors associated with increased risk of DOX-induced cardiotoxicity are being over the

age of 65 (13,14), pre-existing cardiovascular diseases (13), gender as females are at a higher risk (15,16) and DOX dosage. The total cumulative dose is the most critical risk factor in predicting a patient's likelihood of developing DOX-induced cardiotoxicity. About 5% of adult patients experience congestive heart failure when receiving a cumulative dose of 400 mg/m^2 (14). The percentage increases to 26% when the cumulative dose is 550 mg/m^2 and further increases to 48% at a dose of 700 mg/m^2 (14). Even many years after stopping their DOX treatment, patients can still develop DOX-induced cardiotoxicity and its associated cardiovascular complications (12).

1.1.3 Treatment Options for DOX-induced cardiotoxicity

Patients with DOX-induced cardiotoxicity have been treated with drugs such as Dexrazoxane, angiotensin-converting enzyme (ACE) inhibitor, β-blockers, and statins. The only US Food and Drug Administration and Health Canada approved treatment for DOX-induced cardiotoxicity is Dexrazoxane (17). Dexrazoxane functions a chelating agent to reduce the metal ions that form with anthracyclines, thus reducing the generation of ROS (18). However, it has been indicated that Dexrazoxane increases the risk of developing a secondary malignancy in pediatric patients (19). A randomized placebo-controlled study found that ACE inhibitor, Enalapril reduced the early onset of cardiac toxicity in children (20). Also, β-blockers have shown to be effective in preventing DOX-induced cardiotoxicity in patients. For example, Carvedilol prevented the decline of left ventricular ejection fraction in cancer patients (21). Statins can decrease oxidative stress and inflammation caused by DOX. Breast cancer patients on statins had a lower risk of heart failure compared to the non-statin treated group (22). However, the long-term use of ACE inhibitors and β-blockers is associated with an increased risk of cancer occurrence (23,24). More evidence about the success of these drugs is required to fully understand their protective effects in patients.

1.1.4 DOX-induced cardiotoxicity's mechanism of action

The exact mechanism in DOX-induced cardiotoxicity remains unknown. Multiple mechanisms that have been reported to contribute to the development of DOX-induced cardiotoxicity including generation of ROS (25), disruption of calcium ions (26), and impairment of mitochondrial function (27). However, it has been suggested that ROS or

oxidative stress may not be the primary mechanism leading to DOX-induced cardiotoxicity (28). The precise molecular mechanism responsible remains unknown, which makes it difficult to treat patients suffering from these cardiovascular complications.

An emerging mechanism that has been proposed is the dysregulation in autophagy leading to DOX-induced cardiotoxicity. Autophagy is a degradation process that functions to engulf damaged protein and cellular organelles into an autophagosome (29). Autophagic flux refers to the entire process that starts with the formation of autophagosome, fusion with lysosomes to create autolysosomes, and breakdown of molecules (29). A recent study suggests that DOX blocks autophagy by increasing the lysosomal pH to become more basic, which disrupts the breakdown of unwanted cargo in the autolysosomes (30). The accumulation of undegraded cargo leads to increased ROS and results in cardiomyocyte death. By inducing autophagy, it should maintain cardiomyocytes viability after DOX treatment (30). However, the literature presents conflicting reports that DOX can induce excessive autophagy by upregulating initiation genes (31,32). While others have demonstrated that inhibition of autophagy results in increased ROS and accumulation of autolysosome leading to DOX-induced cardiotoxicity (30,33,34). Thus, the involvement of autophagy and DOX-induced cardiotoxicity is not clearly understood.

1.2 Nicotinamide adenine dinucleotide

Nicotinamide adenine dinucleotide (NAD^+) is a pyridine nucleotide that is an essential cofactor and substrate for multiple cellular processes (Figure 2). NAD^+ is found in all cells and plays a role production of cellular energy (adenosine triphosphate [ATP]), glycolysis, and mitochondrial respiration (35). NAD^+ can be produced from nicotinamide (NAM), nicotinic acid, nicotinamide riboside (NR), and nicotinamide mononucleotide (NMN).

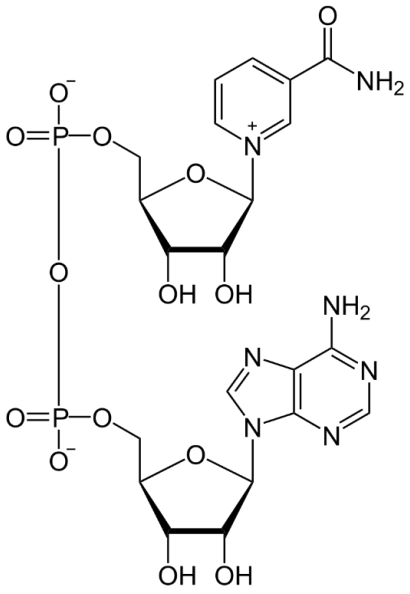

Figure 2: Chemical structure of NAD^+.

The chemical formula of NAD^+ is $C_{21}H_{27}N_7O_{14}P_2$ and the molecular weight is 663.43 g/mol. Figure from Wikimedia Commons (36).

NAM is a water-soluble amide form of vitamin B3 and is a precursor to NAD^+ (37). Nicotinic acid (also known as niacin) is also a form of vitamin B3 that is available in food and supplements. Among the molecules that can synthesize NAD^+, nicotinic acid and NAM have several disadvantages compared to NR and NMN. Nicotinic acid and NAM are associated with flushing (38) and may not activate sirtuins (39). Therefore, NAM or nicotinic acid is not ideal as a therapeutic for patients. Also, NMN and NR are preferred over the administration of NAD^+ because NAD^+ is less soluble and does not effectively pass through the plasma membrane (40).

Many studies have shown that boosting NAD^+ helps to combat diseases such as age-related diseases (41) and diabetes (42). NAD^+ is involved in regulating signalling pathways for NAD^+ dependent enzymes such as sirtuins (SIRTs) and Poly (ADP-ribose) polymerase (PARP) enzymes (35). However, the role of NAD^+ in cardiovascular health has not been intensively investigated (43) despite that the concentration of NAD^+ present in the heart is the second highest, after the liver (44,45).

1.2.1 Salvage NAD^+ Pathway

NAD^+ can be synthesized through 3 different pathways in mammalian cells. The first is the *de novo* pathway which synthesizes NAD^+ from tryptophan. The second pathway is the salvage pathway that produces NAD^+ from NAM, nicotinic acid, NR, or NMN. Lastly, the Preiss-Handler pathway uses nicotinic acid and nicotinate phosphoribosyltransferase (NAPRT) enzyme (46). In the heart, the majority of NAD^+ is synthesized through the salvage pathway (44,46) (Figure 3).

The salvage pathway recycles NAM from NAD^+ consuming enzymes including SIRTs, PARPs, and cyclic ADP-ribose synthases (CD38 and CD157) to produce NAD^+ (47). Nicotinamide phosphoribosyltransferase (NAMPT) recycles NAM into NMN, then NMN is converted into NAD^+ by various nicotinamide mononucleotide adenylyl transferases (NMNATs) including NMNAT 1 in the nucleus, NMNAT 2 in the cytoplasm, and NMNAT 3 in the mitochondria (47,48). NR enters the mammalian cell by equilibrative nucleoside transporters (ENTs) and nicotinamide riboside kinases (NRK1/2) phosphorylates NR into NMN (49–51). Then NMN gets converted into NAD^+ by NMNAT 1/2/3 in the body (49). Two mechanisms have been proposed for the conversion of NMN to NAD^+. First, the conversion of NMN into NAD^+ requires a dephosphorylation step by CD73 to convert into NR before entering the cell due to its larger size, then converted into NMN by NRK1/2 (50). However, a recent study found that the Solute carrier family 12 member 8 (Slc12a8) transporter allows for NMN to be facilitated into the cell without being converted into NR by CD73 or NRK1/2 (52).

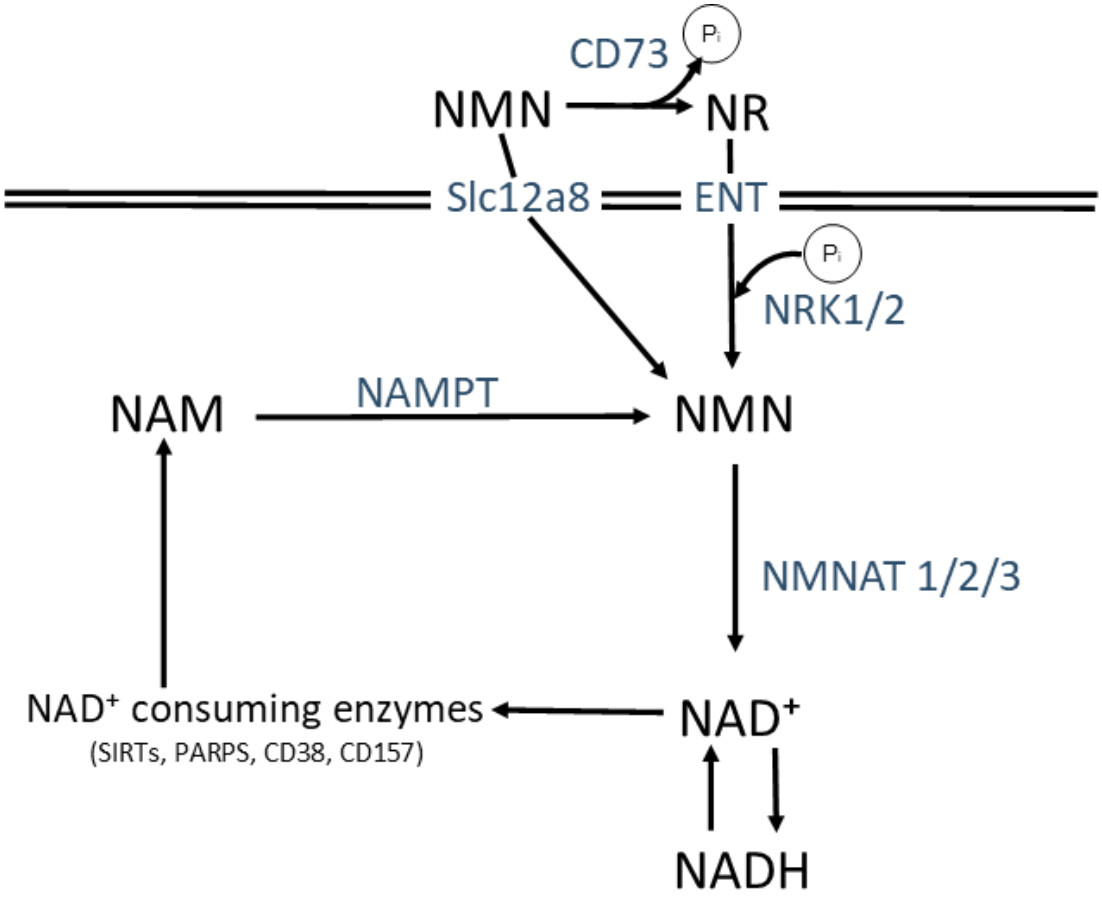

Figure 3: The salvage pathway to synthesizing NAD^+.

The salvage pathway that produces NAD^+ from NR, NMN, or NAM and the enzymes involved (blue). NR can be transported into the cell by ENTs and converted NMN by NRK1/2. Once converted into NMN, it is converted into NAD^+ by NMNAT 1/2/3. NMN can be transported into the cell through the Slc12a8 transporter, then converted into NAD^+ by NMNAT 1/2/3.

1.2.2 Nicotinamide Riboside

NR is a derivate of Vitamin B3 and transported into cells by ENTs (Figure 4). NR has been reported to attenuate heart failure in mice by stabilizing NAD^+ levels (53). In humans, chronic oral NR supplementation effectively stimulated NAD^+ metabolism, reduced systolic blood pressure, and aortic stiffness (53). Also, pre-treatment with NR protected against DOX-induced cardiotoxicity (54). After 24 hours of DOX treatment on cardiomyocytes, there was increased caspase-3 activity, increased DNA fragmentation indicating apoptosis, increased lactate dehydrogenase (LDH) release, and decreased cell viability seen with DOX treatment (54). With the pre-incubation of NR for 24 hours

before DOX treatment, the effects of DOX were lower compared to DOX treatment alone (54). Furthermore, NR attenuated defects in myocardial function in DOX-injected mice in a dose-dependent manner, which supports the indication of cardioprotective effects of NR seen in the *in vitro* findings.

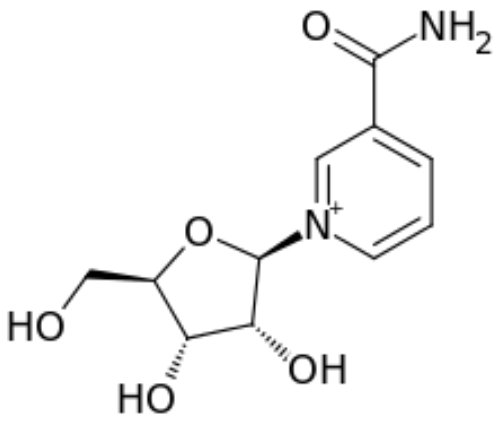

Figure 4: Chemical structure of NR.

The chemical formula of NR is $C_{11}H_{15}N_2O_5$ and the molecular weight is 255.25 g/mol. Figure from Wikimedia Commons (55).

1.2.3 Nicotinamide Mononucleotide

NMN is another intermediate in NAD^+ biosynthesis that can be produced from NAM and phosphoribosyl pyrophosphates in cells (Figure 5). NMN is a source of cellular energy and has a diverse range of functions, including cardioprotection and metabolism regulation (48). NMN has its' own advantage with several successful outcomes where NR failed. For example, NMN treatment on Friedreich's ataxia knockout mice improved diastolic function compared to saline control by increasing Silent mating type information regulation 2 homolog 3 (SIRT3) activity (56). Exogeneous NMN protected the heart against ischemia and reperfusion by decreasing FoxO1 acetylation and through activating the Silent mating type information regulation 2 homolog 1 (SIRT1) pathway (57). Also, it has been reported that NMN has a specific transporter, Slc12a8 that allows for effective uptake into the circulation and tissues (52). A study revealed that NMN increases heart tissue NAD^+ to ameliorate DOX-induced dysfunction and improve

myocardial dysfunction in p53 deficient mice (58). However, NMN has not been extensively studied as a preventive treatment against DOX-induced cardiotoxicity.

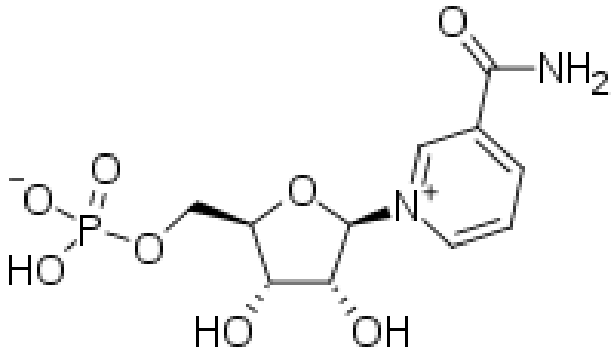

Figure 5: Chemical structure of NMN.

The chemical formula of NMN is $C_{11}H_{15}N_2O_8P$ and the molecular weight is the 334.22 g/mol. Figure from Wikimedia Commons (59).

1.3 Histone Deacetylase Family

Histone deacetylases (HDACs) are enzymes that function to remove acetyl groups from histones. The removal of the acetyl groups increases the positive histone tails to promote high-affinity binding between histone and the DNA backbone (60). HDACs can have an effect on non-histone proteins such as transcription factors (61). There are 18 mammalian HDACs that are categorized into 4 different classes. First, Class I HDACs include HDAC 1, 2, 3, and 8, which have a Zinc dependent mechanism to deacetylase acetyl substrates (62,63). The second group is Class II HDACs including HDACs 4, 5, 6, 7, 9, and 10, which also utilize a Zinc dependent mechanism. Class II HDACs can be categorized into 2 subgroups, where are Class IIa including HDACs 4,5,7, and 9. The other subcategory is Class IIb containing HDAC 6 and 10. The difference is that Class IIa has a large C-terminus while Class IIb contains 2 deacetylase domains. Class III HDACs contain SIRTs 1-7, which are NAD^+ dependent and requires NAD^+ to transfer the acetyl group. The last category is Class IV that only contains HDAC 11 and it is Zinc dependent (62,63).

1.3.1 SIRT1 and DOX-induced cardiotoxicity

SIRT1 and SIRT3 play an important role in maintaining cardiovascular physiology (64–66). SIRT1 and SIRT3 functions as NAD^+ dependent class III histone deacetylases. Specifically, SIRT1 is highly expressed in cardiomyocytes and the NAD^+/SIRT1 signaling pathway plays roles in metabolism, cellular energy maintenance, and longevity (67). DOX decreased SIRT1 expression leading to DOX-induced myocardial apoptosis (68). Pre-treatment with Resveratrol inhibited DOX-induced apoptosis in H9c2 cells through activation of SIRT1 (68). The administration of the SIRT1 inhibitor (EX-527) eliminated the protective effect of NR (54). This suggests that DOX interferes with SIRT1's regulation and the conversion of NR into NAD^+ activates SIRT1 to provide protection.

1.3.2 SIRT3 and DOX-induced cardiotoxicity

DOX treatment suppressed cardiac SIRT3 expression and is associated with higher protein acetylation levels in H9c2 cells (64). Furthermore, overexpression of SIRT3 protected cardiomyocytes from DOX induced cell death (64). The mechanism of SIRT3 involves activation of NAD^+ which alleviates hyperacetylation and attenuated cardiac dysfunction (69). Therefore, HDAC specifically NAD^+ consuming enzymes SIRTs plays an important role in the development of DOX-induced cardiotoxicity.

1.4 Histone Acetyltransferase Family

The balance between acetylation and deacetylation is critical in maintaining various cellular processes (70). Studies have proposed that the disbalance between histone acetyltransferases (HATs) and HDACs activity contributes to cancers (71), inflammatory diseases (72), and neurodegenerative disease (73). The increase in acetylation of various molecular components has highlighted the importance of post-translational modifications in DOX-induced cardiotoxicity. For example, DOX triggers increased p53 lysine acetylation through the DNA damage repair pathway, thus upregulating p53 activity (74). It has been observed that DOX decreases HDAC activity in cardiomyocytes and resulted in increased p53 acetylation (54,75). When H9c2 cells were pre-treated with Trichostatin A (TSA), a global HDAC inhibitor, it augmented DOX-induced cardiac hypertrophy and DNA stranded breaks (61,76). Thus, the balance between acetylation and deacetylation is

critical for cell survival in DOX-induced cardiotoxicity. However, the role of the HAT family members has not been identified in DOX-induced cardiotoxicity.

HATs are enzymes on chromatin structures involved in transcription activation through loosening chromatin to neutralize positively charged lysine. HATs are enzymes that function to add an acetyl group on histone and non-histone proteins (77). HATs are categorized into 2 types, Type A HATs and Type B HATs. Type A HATs are mainly nuclear and can be subclassified into 5 groups. The first group is the GCN5-related acetyltransferases (GNAT) containing General Control Nonderepressible (GNC5), p300/CBP associated factor (PCAF), and Elongator complex protein (ELP3). The second group is p300/CBP consisting of p300 and CREB-binding protein (CBP). The third group is called the MOZ, YBF2/SAS3, SAS2, and TIP60 protein (MYST) family containing MYST1 (HMOF), MYST2 (HB01), MYST3 (MOZ), MYST4 (MORF) and tat interacting protein 60 kDa (TIP60). The fourth group is the basal Transcription factor family including Transcription Factor IIIC and Tat-interactive protein 60 kDa (TAF1). Lastly are the nuclear receptor cofactors (NRCF) family with steroid receptor coactivator (SRA) and nuclear receptor coactivator 3 (NCOA3/ACTR) (78).

Type B HATs are referred to as cytoplasmic HATs because they are responsible for modifying free histone in the cytoplasm. The family contains HAT1, HAT2, Rtt109, HatB3.1, and HAT4 (78). Specifically, Type A HATs are of interest because of their ability to function as acetyltransferase for histone and non-histone targets including SIRT2 (79).

1.4.1 GCN5 and Butyrolactone 3 inhibitor

GCN5/PCAF can acetylate non-histone proteins such as tumour suppressors (80) and numerous transcription factors (81). It contains a HAT domain that is about 160 resides with a conserved bromodomain (82). One of the HAT inhibitors used in this study is Butyrolactone 3, which is a GCN5 inhibitor with an IC_{50} value of 100 μM (Figure 6) (4). Butyrolactone 3 (also called MB-3) inhibits HAT GCN5 and derived from γ-

Butyrolactones, class of metabolites from the Aspergillus genus (83). There are no published studies examining the effect of Butyrolactone 3 in cardiovascular research.

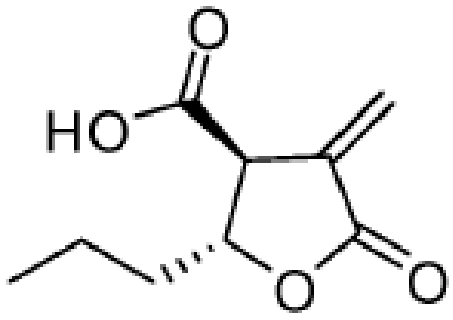

Figure 6: Chemical structure of Butyrolactone 3.

The chemical formula of Butyrolactone 3 is $C_9H_{12}O_4$ and the molecular weight is 184.19 g/mol. Figure from Mai *et al*., (84).

1.4.2 TIP60 and MG149 inhibitor

TIP60 is a member of the MYST family and plays a critical role in a wide range of cellular processing such as cell growth and transcription (85). TIP60 protein is required for cardiomyocyte vitality and survival (86). Also, TIP60 is highly expressed in cardiomyocytes and contributes to autophagy regulation (87). To identify the role of TIP60 in this study, we used MG149, a TIP60 inhibitor at an IC_{50} values of 74 μM (88) (89) derived from anacardic acid (90) (Figure 7).

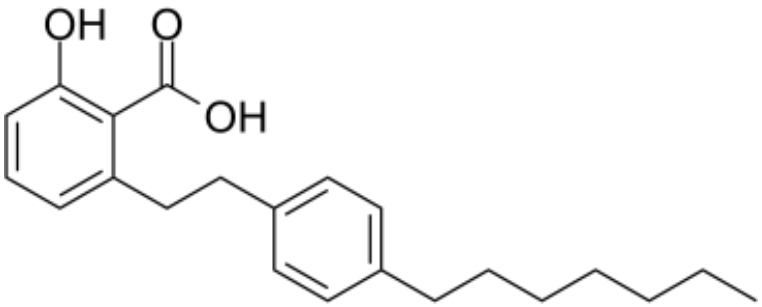

Figure 7: Chemical structure of MG149.

The chemical formula for MG149 is $C_{22}H_{28}O_3$ and the molecular weight is 340.46 g/mol. Figure from MedChemExpress (91).

1.4.3 p300/CBP, C646, and HAT inhibitor II

The p300/CBP family consists of related proteins p300 and CBP, which have a similar structure containing a HAT domain that is about 500 residues with 86% sequence identity, a bromodomain, and 3 cysteine-histidine rich domains (92). p300 and CBP are involved in physiological processes including cell survival, maintaining cardiac mitochondrial function (93), differentiation, and growth of cardiomyocytes (94). A study revealed that HAT inhibitor, Spermidine was able to induce autophagy by inhibiting p300 activity which was associated with decreased acetylation levels and increase autophagic flux (95).

In this study, we used HAT inhibitor II, which is a novel selective inhibitor for p300 (Figure 8) (96). HAT II inhibitor is a cyclohexanone derivative and inhibits p300 with IC_{50} values ranging from 5-233 μM (96). Another small molecule inhibitor for p300/CBP used in this study is C646 with an IC_{50} value of 1.6 μM (Figure 9) (97). A diagram of the HAT inhibitors used in this study and its associated HAT target can be seen in Figure 10.

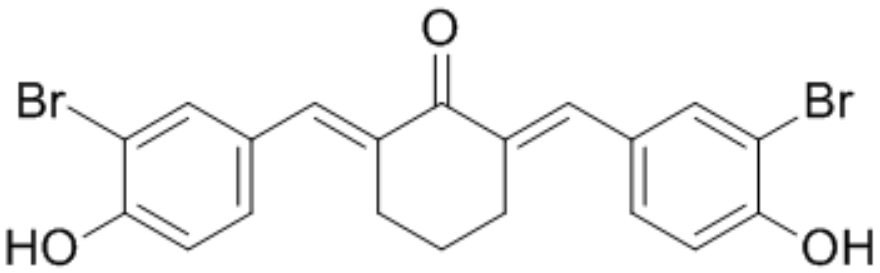

Figure 8: Chemical structure of HAT inhibitor II.

The chemical formula of HAT inhibitor II is $C_{20}H_{16}Br_2O_3$ and the molecular weight is 464.15 g/mol. Figure from Costi *et al*., (96).

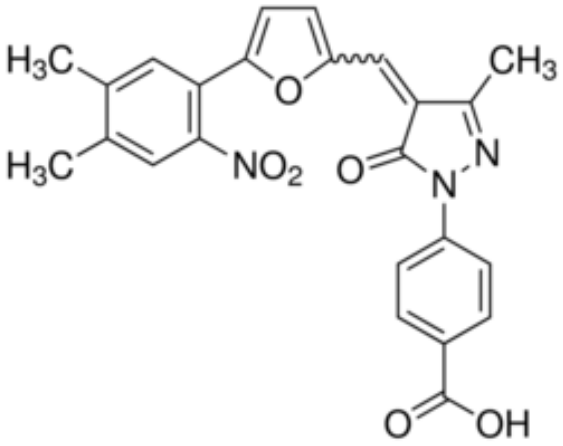

Figure 9: Chemical structure of C646.

The chemical formula of C646 is $C_{24}H_{19}N_3O_6$ and the molecular weight is 445.42 g/mol. Figure from Bowers *et al*., (97).

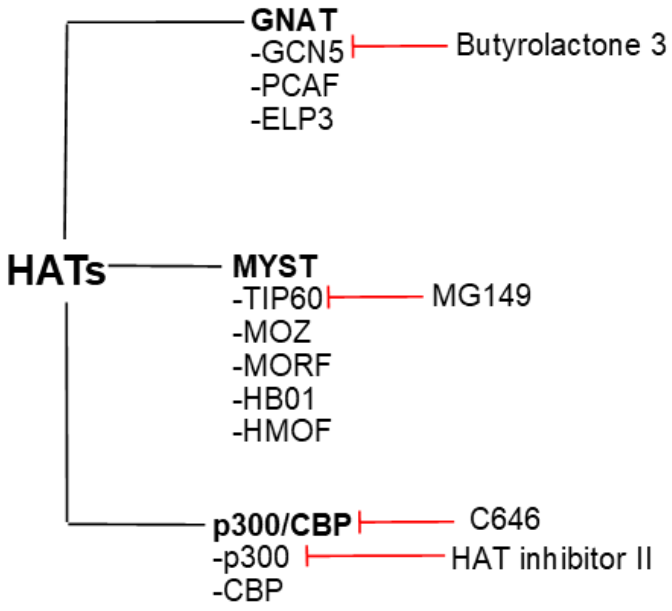

Figure 10: Diagram of the HAT family members and inhibitors used in this study.

The pharmacological inhibitors that have been used in this study shown to inhibit the targeted HAT family member.

Table 1: Summary of the chemical structure, formula, and function of key biological and chemical molecules.

Name	Chemical Structure	Molecular Weight (g/mol)	Function
DOX	$C_{27}H_{29}NO_{11}$	543.56	Chemotherapy
NAD^+	$C_{21}H_{27}N_7O_{14}P_2$	663.43	Cofactor involved in various cellular processes
NR	$C_{11}H_{15}N_2O_5$	255.25	Precursor to NAD^+
NMN	$C_{11}H_{15}N_2O_8P$	334.22	Precursor to NAD^+
Butyrolactone 3	$C_9H_{12}O_4$	184.19	GCN5 inhibitor
MG149	$C_{22}H_{28}O_3$	340.46	TIP60 inhibitor
HAT inhibitor II	$C_{20}H_{16}Br_2O_3$	464.15	p300 inhibitor
C646	$C_{24}H_{19}N_3O_6$	445.42	p300/CBP inhibitor

1.5 Proposed Model

We proposed that DOX-induced toxicity onto cardiomyocytes by reducing NAD^+ concentration in the cells (Figure 11). The low concentration of NAD^+ impacts SIRTs' activity leading to increased acetylation levels in the cells. The increased acetylation impairs autophagy and is associated with the accumulation of undegraded cargo. Thus, it results in cardiomyocyte cell death. By increasing NAD^+ with NMN, SIRTs activity will increase, thereby prevent acetylation and protection from cell death. Alternatively, preventing acetylation using a small molecular HAT inhibitor can decrease acetylation levels to prevents cardiomyocytes cell death.

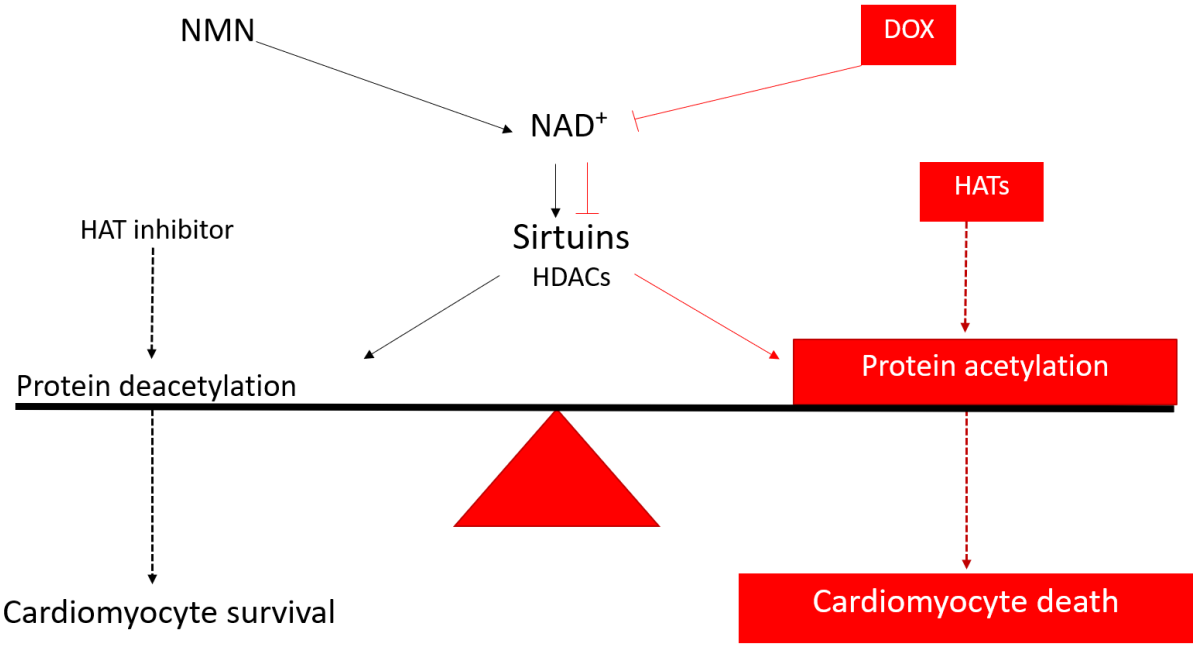

Figure 11: Proposed Model of DOX-induced cardiotoxicity.

DOX impacts NAD^+ concentration in cardiomyocytes. The low concentration of NAD^+ impacts SIRTs' activity leading to increased protein acetylation levels in the cells. The increased acetylation impairs autophagy and eventually results in cardiomyocyte cell death. By increasing NAD^+ with NMN, SIRTs activity will increase thereby prevent acetylation and protecting cells from death.

1.6 Hypothesis

It is hypothesized that administrating NMN to increase cellular NAD^+ concentration or HAT inhibitors to prevent protein acetylation will protect cells against DOX-induced cardiotoxicity.

1.7 Specific Aims

1.7.1 To evaluate the utility of H9c2 cell culture as an *in vitro* model to study DOX-induced cardiotoxicity

Rationale for Aim 1: The H9c2 cell line was derived from embryonic rats' ventricular heart tissue. The H9c2 cells exhibit similar membrane morphology and electrophysiological properties to primary cardiomyocytes (98). The purpose of this objective is to confirm the utility of H9c2 cell culture to study DOX-induced cardiotoxicity and to ensure that DOX induces H9c2 cell death in a dose-dependent manner.

1.7.2 To determine if NMN protects against DOX-induced cardiotoxicity through boosting cellular NAD^+ concentration in H9c2 cells and adult mice hearts

Rationale for Aim 2: Our laboratory revealed that the administration of NR prevented DOX-induced cardiotoxicity (54). The protective effect of NR involved converting into NAD^+, then activation of SIRT1 to prevent DOX-induced cardiotoxicity in both neonatal cardiomyocytes and adult mouse tissue (54). To further investigate the role of NAD^+ and the other NAD^+ precursors, I administered NMN to determine if NMN can protect against DOX-induced cardiotoxicity on H9c2 cells and adult mice.

1.7.3 To examine the effect of pharmacological HAT inhibitors on DOX-induced cardiotoxicity

Rationale for Aim 3: Our previous research revealed that DOX interferes with SIRTs regulation and inhibition of HDAC with TSA increased DOX damage (75). Since HDACs are involved in protecting against DOX-induced cardiotoxicity, I aim to determine if HATs are involved in this process. Therefore, the goal of this objective is to

examine if HAT inhibitors play a role in protecting against DOX-induced damage in H9c2 cells.

Chapter 2

2 Material and Methods

2.1 Cell Culture

The H9c2 cell line was purchased from the American Type Culture Collection. H9c2 cells were grown and maintained in High Glucose Dulbecco's Modified Eagle Medium (DMEM; Gibco, Waltham, Massachusetts), 1% penicillin-streptomycin (P/S, 10000 IU penicillin, 10000 μg/mL streptomycin; Gibco, Waltham, Massachusetts), and 10% heat-inactivated fetal bovine serum (FBS; Thermo Fisher Scientific, Waltham, Massachusetts) at 37°C in a 5% CO_2 incubator.

When passaging the cells, 3 mL of D-Hank's solution (Table 2) was used to wash the cells for 30 seconds at room temperature. Then, 1.5 mL of 0.25% Trypsin (2.21 mM EDTA; Wisent Bioproducts, Saint-Jean-Baptiste, Quebec) was added into the flask and placed into the 37°C incubator for 60 seconds. Six mL of DMEM containing 1% P/S and 10% FBS was added into the flask to terminate the trypsinization process. After terminating the trypsinization, cells were collected into a 12 mL tube and centrifuged at 200 rpm for 5 minutes.

When seeding the cells, the same steps for passaging the cells were performed. The supernatant was removed and 6 mL of fresh DMEM containing 1% P/S and 10% FBS at 37°C was added into the flask. Cells were counted using a hemocytometer for the subsequent assays.

For cell cryopreservation, cells were passaged and the supernatant was removed. Then 900 μL of 10% FBS and 100 μL of dimethyl sulfoxide (DMSO; Bio Basic, Markham, Canada) were added into the 12 mL tube. A transfer pipette was used to suspend the cell in the solution. The solution was transferred into a 1.5 mL tube and placed into a -80°C freezer. To thaw cells, the frozen 1.5 mL tube containing

cells was removed from the -80°C freezer and placed into a 37°C water bath for 30 seconds. Then, the solution was added into a T25 flask with 5 mL of DMEM containing 1% P/S and 10% FBS.

Table 2: Components in 1L of D-Hanks' solution

Component	Amount
D-Glucose	1.000 g
Potassium chloride (KCl)	0.400 g
Potassium Dihydrogen Phosphate (KH_2PO_4)	0.060 g
Sodium chloride (NaCl)	8.000 g
Phenol red	0.012 g

2.2 Caspase-3 Activity Measurement

Caspase-3 activity was measured as an indicator of apoptosis after cell treatment. The culture media in each well was removed, then 100 μL of lysis buffer (Table 3) was added into each well. A cell scraper was used to detach cells from the plate. The cells were collected into 1.5 mL tubes and centrifuged at 10,000 rpm for 7 minutes at 4°C. The Bradford assay was used to determine the protein concentration of the supernatant. Afterward, in a 96-black well plate, 150 μg of protein was incubated in the assay buffer (Table 4) with Ac-DEVD-AMC (Cayman Chemical, Ann Arbor, Michigan) and Ac-DEVD-CHO (Cayman Chemical, Ann Arbor, Michigan) or Ac-DEVD-AMC only for 3 hours at 37°C. The measurement for caspase-3 activity was recorded on a fluorescent spectrophotometer every 30 minutes for 4 hours at an excitation of 355 nm and an emission of 460 nm. Caspase-3 activity is measured as fluorescence intensity values and presented as relative fold changes to the control value in the results.

Table 3: Components in 100 mL of Caspase-3 Lysis Buffer.

Component	Amount/Volume
CHAPS	0.1 g
DTT	500.0 µL
EDTA	20.0 µL
HEPES (pH 7.4)	5.0 mL
NP-40	100.0 µL
H_2O	94.4 mL

Table 4: Components in 100 mL of Caspase-3 Assay Buffer.

Component	Amount/Volume
CHAPS	0.1 g
DTT	1.0 mL
EDTA	200.0 µL
Glycerol	10.0 mL
HEPES (pH 7.4)	5.0 mL
NaCl	585.0 mg
H_2O	83.8 mL

2.3 Lactate Dehydrogenase Release Assay from Clontech

The colorimetric kit was used according to the manufacturer's instructions (Clontech, Mountain View, California) to detect LDH activity released in the supernatant when NAD^+ was reduced to $NADH^+$. For each well, 50 µL of the sample and 50 µL of the LDH reaction mixture were added into a transparent 96-well plate. Readings were taken after 15 minutes of adding the reaction mixture and measured at 490 nm in a microplate reader. LDH release is measured as absorbance values and presented as relative fold changes to the control value in the results.

2.4 NAD^+ Microplate Reader Assay from Cohesion Biosciences

To detach and collect the cells for the NAD^+ concentration assay, 500 µL of 0.25 % Trypsin was added into each well for 30 seconds. Then, 1.5 mL of DMEM with 1% P/S and 10% FBS was added into each well to terminate the trypsinization process. Cells were collected into a 2 mL tube and centrifuged at 1000 rpm for 5 minutes at 4°C. The supernatant was removed, then the NAD^+ concentration was

extracted and measured according to the NAD/NADH Microplate Assay Kit manufacturer's instructions (Cohesion Biosciences, Burlington, Ontario). The readings for the assay were measured at 550 nm using a microplate reader. NAD^+ concentration is measured as absorbance values and presented as relative fold changes to the control value in the results.

2.5 Caclein AM Cell Viability Assay from Trevigen

To assess cell viability, 2 washes of 100 µl of 1X calcein AM DW Buffer was performed before 1 µM calcein was used to stain the cells. All other steps of the assay were used following to manufacturers' instructions (Trevigen, Gaithersburg, Maryland). The readings were measured every 10 minutes for 30 minutes using a fluorescent spectrophotometer at 480 nm excitation and 520 nm emission. Calcein AM cell viability is measured as fluorescence intensity values and presented as relative fold changes to the control value in the results.

2.6 Animals

Experimental procedures were approved by the Animal Use Subcommittee at the University of Western in Ontario, Canada (Animal Use Protocol #2016-059). The animal studies were conducted at Victoria Research Laboratories of Lawson Health Research Institute. The breeding pairs of C57BL/6 mice were purchased from the Jackson Laboratory. All animals were housed in a temperature and humidity-controlled facility with water and food.

2.7 Echocardiography

We established 4 groups including vehicle control, NMN control, DOX vehicle, and NMN with DOX group. Each group contained 5 three-month-old C57BL/6 male mice reared under the same conditions. Mice were injected with either NMN (500 mg/kg, i.p.) or saline. Thirty minutes later, the mice received a DOX (20 mg/kg, i.p.) or saline injection. After 5 days, animals were anesthetized with 1% inhaled isoflurane. Then, the mice were placed into handling platform and imaged with a 40-MHz linear array transducer using a pre-clinical ultrasound system (Vevo 2100, Visual Sonics, Canada) and nominal in-plane spatial resolution of 40 µM (axial) by 80 µM (lateral). Pulsed wave

Doppler measures of maximal early and late transmitral velocities in diastole were collected at the apical view (cursor at mitral valve inflow). The changes to the LVIDd, LVIDs, ejection fraction (EF) percentage, and fractional shortening (FS) percentage was analyzed on M-mode scans at the 2D parasternal short axis.

The EF is the volumetric fraction of blood pumped from the left ventricle (LV) at each beat. The EF% is calculated by the equation,

$$EF\% = \left(\frac{LV\ diastolic\ volume - LV\ systolic\ volume}{LV\ distolic\ volume}\right) x100$$

The FS is the measurement of change in the LV diameter. The FS % is calculated by the equation,

$$FS\% = \left(\frac{LVIDd - LVIDs}{LVIDd}\right) x100$$

2.8 Evans Blue Staining

Four groups including vehicle control, NMN control, DOX vehicle, and NMN with DOX group was established. Each group contained 5 three-month-old C57BL/6 male mice. Mice were injected with either NMN (500 mg/kg, i.p.) or saline. After 30 minutes, the mice received a DOX (20 mg/kg, i.p.) or saline injection. Five days later, Evan Blue dye (100 mg/kg, i.p.) was dissolved in 1X Phosphate-buffered saline (PBS; Table 5), then injected into all of the mice. Four hours later, mice were euthanized by cervical dislocation and the hearts were collected. The hearts were embedded into the optimal cutting temperature compound (Sakura Finetek, Torrance, California) and placed into a -80°C freezer. The frozen tissue was cut into 6 μM thickness cryosections, stained with 8 μL of 1 mg/mL of Hoechst 33342 (Invitrogen, Carlsbad, California) for 20 minutes, and mounted with 10 μL fluorescence mounting medium (Agilent Technologies Santa Clara, California).

Cell membrane permeability to Evans Blue dye was visualized under a fluorescence microscope and positive cells were captured on 10x and 40x objective. The percentage of positive cell staining was estimated using 20 different images for each treatment group (5 samples x 4 images per sample; totaling at least 6000 nuclei) captured on 10x with the ImageJ software. The results are presented as the estimated percentage of positive cells stained with Evan Blue relative to the total nuclei stained.

Table 5: Components in 1L of 1X PBS.

Component	Amount/Volume
KCl	0.20 g
KH_2PO_4	0.24 g
NaCl	8.00 g
Sodium Phosphate Dibasic (Na_2HPO_4)	1.44 g
H_2O	995 mL

2.9 Solution preparation

2.9.1 DOX

A stock concentration of 1 mM DOX was created by dissolving 0.0011 g of DOX (Hospira, London, Ontario) into 2 mL of sterilized H_2O. The solution was mixed until it was uniformly distributed. The stock solution was stored at 4 °C for up to 1 month. The working concentration of DOX (1, 2, or 5 μM) was created using 1 mM of DOX and diluted with DMEM containing 1% P/S and 10% FBS.

2.9.2 NMN

A stock concentration of 10 mM NMN was created by dissolving 0.001 g of NMN (Apexbio Technology, Burlington, Ontario) into 299 μL of sterilized H_2O. The solution was mixed until it was evenly distributed. The stock solution was stored at -20°C for up to 6 months. The working concentration of 500 μM NMN was created using the 10 mM of NMN and diluted with DMEM containing 1% P/S and 10% FBS.

2.9.3 NAD^+ free acid

A stock concentration of 10 mM NAD^+ free acid was created by dissolving 0.0019 g of NAD^+ free acid (Calbiochem, Oakville, Ontario) into 286 µL of sterilized H_2O. The solution was mixed until it was uniformly distributed. The stock solution was stored at -20°C for up to 6 months. The working concentration of 500 µM NAD^+ free acid was created using the 10 mM of NAD^+ free acid and diluted with DMEM containing 1% P/S and 10% FBS.

2.9.4 Butyrolactone 3

A stock concentration of 200 mM Butyrolactone 3 was created by dissolving 5 mg of Butyrolactone 3 (Cayman Chemicals, Ann Arbor, Michigan) into 135 µL of DMSO (Bio Basic, Markham, Canada). The solution was mixed until it was uniformly distributed. The stock solution was stored at -20°C for up to 12 months. The working concentration of (50 or 100 µM) Butyrolactone 3 was created using the 200 mM of Butyrolactone 3 and diluted with DMEM containing 1% P/S and 10% FBS.

2.9.5 MG149

A stock concentration of 10 mM MG149 was created by dissolving 1 mg of MG149 (Cayman Chemicals, Ann Arbor, Michigan) into 293 µL of DMSO (Bio Basic, Markham, Canada). The solution was mixed until it was evenly distributed. The stock solution was stored at -20°C for up to 12 months. The working concentration of 10 µM MG149 was created using the 10 mM of MG149 and diluted with DMEM containing 1% P/S and 10% FBS.

2.9.6 C646

A stock concentration of 10 mM C646 was created by dissolving 1 mg of C646 (Cayman Chemicals, Ann Arbor, Michigan) into 224 µL of DMSO (Bio Basic, Markham, Canada). The solution was mixed until it was evenly distributed. The stock solution was stored at -20°C for up to 12 months. The working concentration of (2, 10, or 30 µM) C646 was created using the 10 mM C646 and diluted with DMEM containing 1% P/S and 10% FBS.

2.9.7 HAT inhibitor II

A stock concentration of 10 mM HAT inhibitor II was created by dissolving 1 mg of HAT inhibitor II (Cayman Chemicals, Ann Arbor, Michigan) into 215 µL of DMSO (Bio Basics, Toronto, Canada). The solution was mixed until it was uniformly distributed. The stock solution was stored at -20°C for up to 12 months. The working concentration of (5 or 10 µM) HAT inhibitor II was created using the 10 mM of HAT inhibitor II and diluted with DMEM containing 1% P/S and 10% FBS.

2.10 Data Analysis

The data are provided as mean values ± SD. A one-way ANOVA analysis followed by the Bonferroni test was performed. All statistical analyses were performed using GraphPad Prism 8. A statistical significance was defined by *p-value ≤0.05, ** p-value ≤ 0.01, ***p-value ≤0.001, and ****p-value≤ 0.0001.

Table 6: List and descriptions of reagents.

Name	Description	Source (Catalog Number)
Ac-DEVD-AMC	Caspase-3 fluorogenic substrate	Cayman Chemicals (14986)
Ac-DEVD-CHO	Caspase 3/caspase-7 inhibitor	Cayman Chemicals (10017)
Bradford Assay	Measure protein concentration	Bio-Rad (500-0001)
Butyrolactone 3	GNC5 inhibitor	Cayman Chemicals (12095)
C646	p300/CBP inhibitor	Cayman Chemicals (10549)
CHAPS	Chemical reagent	Bio Basic (CD0110)
DAKO Fluorescence Mounting Medium	Visualization of specimens	Agilent Technologies (S3023)
D-glucose	Chemical reagent	Bio Basic (GB0219)
DMEM	Cell culture media	Gibco (11965092)
DMSO	Organic reagent	Bio Basic (DC4103)
DOX	Chemotherapy drug	Hospira (02194465)
DTT	Chemical reagent	Bio Basic (DB0058)
EDTA	Chemical reagent	Sigma (E5134)
Evans Blue dye	Non-permeating dye to check cell viability	Invitrogen (314136)
FBS	Growth factors and	Thermo Fisher Scientific

	supplements for cell culture	(16000044)
Glycerol	Chemical substance	Sigma (G5516)
HAT inhibitor II	p300 inhibitor	Cayman Chemicals (19835)
HEPES	Buffering agent	Bio Basic (HB0264)
Hoechst 33342	Nucleic acid stain	Invitrogen (H3570)
KCl	Chemical reagent	Sigma (PX1405-1)
KH2PO4	Chemical reagent	Bio Basic (PB0445)
MG149	TIP60 inhibitor	Cayman Chemicals (22135)
Na_2HPO_4	Chemical reagent	Sigma (S0876)
NaCl	Chemical reagent	Bio Basic (DB0483)
NAD^+ free acid	Chemical cofactor for enzyme	Calbiochem (481911)
NMN	Intermediate of NAD^+	Apexbio Technology (B7878)
NP-40	Detergent	Sigma (13021)
P/S	Antibiotic penicillin and streptomycin	Gibco (15140122)
Phenol red	pH indicator	Sigma (P5530)
Tissue-Tek Optimal cutting temperature compound	Compound to embed tissue sample	Sakura Finetek (4583)
Trypsin	Cell dissociation reagent	Wisent Bioproducts (325-043-EL)

Chapter 3

3 Results

3.1 DOX increases LDH release in a dose-dependent manner

Cell death encompasses different types of cellular processes including necrosis and apoptosis. My first cell death assays involved detecting LDH, which is a cytoplasmic enzyme released into the culture media and a measure of necrosis. I cultured H9c2 cells in 24-well plates at a seeding density of $2.0x10^4$ cells per well, then treated cells with either 1, 2, or 5 μM of DOX for 24 hours. One μM of DOX resulted in higher LDH by approximately 30%, while 2 μM of DOX resulted in higher LDH by 90% compared to the control group. At 5 μM of DOX, there was an increase of 160% in LDH release compared to control (Figure 12). Therefore, DOX induces LDH release in a dose-dependent manner.

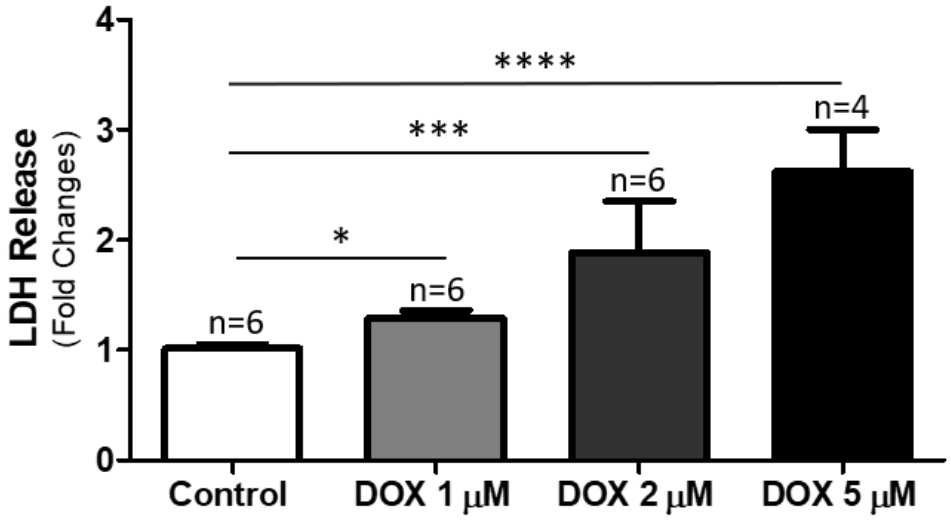

Figure 12: Effect of DOX on LDH release in H9c2 cells.

H9c2 cells were treated with 1, 2, and 5 μM of DOX for 24 hours in culture media. LDH levels were determined from the culture media. Data are provided as means ± SD. A one-way ANOVA analysis followed by the Bonferroni test was performed. A statistical significance was defined by *p-value ≤ 0.05, ***p-value ≤ 0.001, and ****p-value ≤ 0.0001.

3.2 DOX increases caspase-3 activity in a dose-dependent manner

Apoptosis is another method of cell death. To differentiate between necrosis and apoptosis, I detected caspase-3 activity as a measure of apoptosis. I cultured H9c2 cells in 24-well plates at a seeding density of $2.0x10^4$ cells per well, then treated cells with either 1, 2, or 5 μM of DOX for 24 hours. To collect the cells, I added a lysis buffer (Table 3) and scraped the cells off the plate for the caspase-3 activity assay. One μM of DOX resulted in higher caspase-3 activity by approximately 90%, while 2 μM increased caspase-3 activity by 9-fold compared to the control group. At 5 μM of DOX, caspase-3 activity was 14-fold higher than the control group (Figure 13). Therefore, DOX-induced caspase-3 activity in a dose-dependent manner.

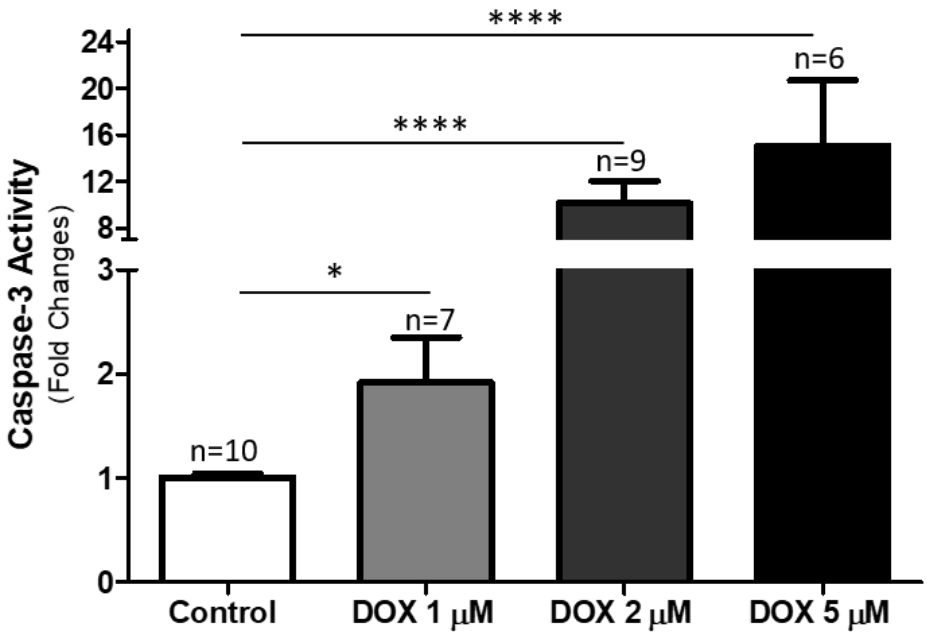

Figure 13: Effect of DOX on caspase-3 activity in H9c2 cells.

H9c2 cells were treated with 1, 2, and 5 μM of DOX for 24 hours in culture media. Apoptosis was determined by caspase-3 activity. Data are provided as means ± SD. A one-way ANOVA analysis followed by the Bonferroni test was performed. A statistical significance was defined by *p-value ≤ 0.05 and ****p-value ≤ 0.0001.

3.3 DOX reduces H9c2 cells viability in a dose-dependent manner

To further understand DOX's effect on H9c2 cells, I determined H9c2 cell viability using calcein AM, a compound that will produce a strong fluorescent compound in live cells. The advantage of utilizing this technique is that I can image the live cell with a fluorescent microscope and capture the quantitative measurement within 2 hours. I cultured H9c2 cells in 96-well plates at a seeding density of $2.0x10^3$ cells per well then treated cells with either 1, 2, or 5 μM of DOX for 24 hours.

The results showed that 1 μM of DOX decreased H9c2 cell viability by 25% compared to the control. While increasing to 2 μM resulted in lower cell viability by 35% compared to the control group. At 5 μM of DOX, cell viability was 40% lower compared to the control (Figure 14). Therefore, DOX decreased H9c2 cell viability in a dose-dependent manner.

My results revealed that DOX induces damage onto H9c2 cells in a dose-dependent manner as determined by the LDH release, caspase-3 activity, and cell viability experiments. Based on these findings, I decided to use 1 μM of DOX for subsequent experiments on H9c2 cells since that dose can induce sufficient damage to H9c2 cells.

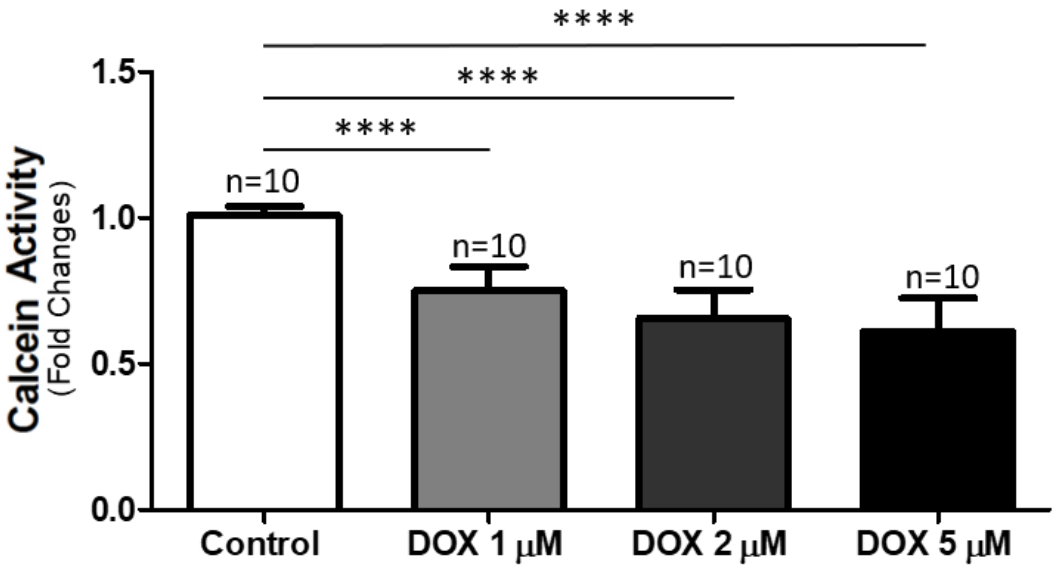

Figure 14: Effect of DOX on H9c2 cells viability.

H9c2 cells were treated with either DOX at 1, 2, and 5 μM on H9c2 cells for 24 hours in culture media. The graph shows the quantitative data of cell viability measured with 1 μM of calcein AM. Data are provided as means ± SD. A one-way ANOVA analysis followed by the Bonferroni test was performed. A statistical significance was defined by ****p-value ≤ 0.0001.

3.4 DOX treatment results in lower NAD^+ concentration in H9c2 cells

To determine the effect of DOX on NAD^+, I measured the NAD^+ concentration after DOX treatment. I seeded H9c2 cells in a 24-well plate at a seeding density of $2.0x10^4$ per well. Then, I pre-incubated the cells with either vehicle or DOX for 24 hours in culture media. After treatment with DOX, I collected the cells and measured the NAD^+ concentration using a commercially available kit from Cohesion Biosciences. I found that the DOX treated group had a 20% lower NAD^+ concentration compared to the control group (Figure 15).

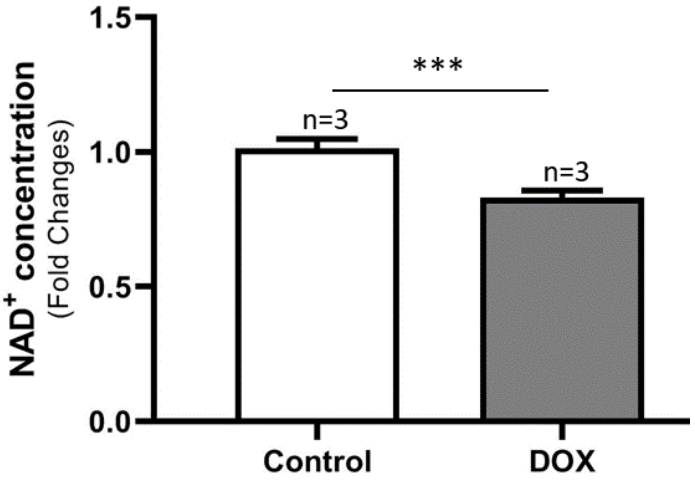

Figure 15: NAD^+ concentration after treatment with DOX in H9c2 cells.

NAD^+ concentration of H9c2 cells after treatment with 1 μM of DOX for 24 hours or 500 μM of NMN for 18 hours in culture media. Data are provided as means ± SD. A one-way ANOVA analysis followed by the Bonferroni test was performed. A statistical significance was defined by ***p-value ≤ 0.001.

3.5 NMN treatment results in higher NAD^+ concentration in H9c2 cells

To ensure that NMN is converted into NAD^+, I measured the NAD^+ concentration after NMN treatment. I seeded H9c2 cells in a 24-well plate at a seeding density of $2.0x10^4$ per well. Then, I pre-incubated the cells with either NMN (500 μM) or vehicle for 18 hours in culture media. After treatment with NMN, the cells were collected and NAD^+ concentration was measured using a commercially available kit from Cohesion Biosciences. The result revealed that pre-incubating H9c2 cells with NMN resulted in a 17% higher NAD^+ concentration compared to the vehicle treated group (Figure 16).

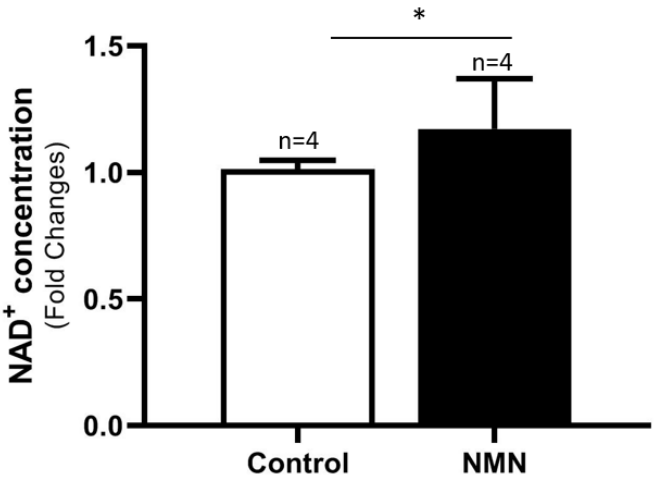

Figure 16: NAD^+ concentration after treatment with NMN in H9c2 cells.

NAD^+ concentration of H9c2 cells after treatment with 1 μM of DOX for 24 hours or 500 μM of NMN for 18 hours in culture media. Data are provided as means ± SD. A one-way ANOVA analysis followed by the Bonferroni test was performed. A statistical significance was defined by *p-value ≤ 0.05.

3.6 NMN abrogates LDH release in H9c2 cells

I measured the LDH release of cells pre-treated with NMN to determine damage by DOX. I seeded H9c2 cells in a 24-well plate at a seeding density of $2.0x10^4$ cells per well. I pre-incubated cells with either vehicle or NMN for 18 hours, then treated cells with DOX for 24 hours in culture media. After treatment with DOX, I collected supernatant and measured the LDH release. The results revealed that cells treated with 500 μM of NMN had about 30% lower LDH release than DOX treated cells (Figure 17). The level of LDH release in the pre-incubated group with NMN was similar to that in the control group, which suggests that NMN can prevent the increased LDH release caused by DOX.

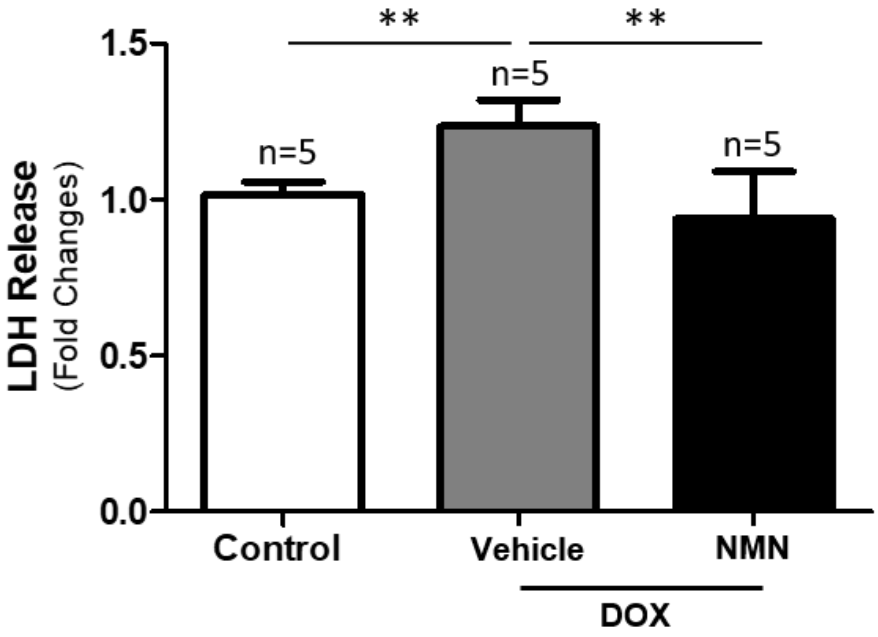

Figure 17: Effect of NMN on LDH release in H9c2 cells.

H9c2 cells pre-incubated with vehicle or 500 μM of NMN for 18 hours in culture media, then 1 μM of DOX for 24 hours. LDH release was determined using the culture media. Data are provided as means ± SD. A one-way ANOVA analysis followed by the Bonferroni test was performed. A statistical significance was defined by **p-value ≤ 0.01.

3.7 NMN abrogates caspase-3 activity in H9c2 cells

I measured caspase-3 activity as an indicator of apoptosis. I seeded H9c2 cells in a 24-well plate at a seeding density of $2.0x10^4$ cells per well. Then, I pre-incubated cells with either vehicle or NMN for 18 hours, then treated cells with DOX for 24 hours in culture media. The results revealed that pre-incubation with 500 μM of NMN before DOX treatment resulted in a 60% reduction in caspase-3 activity compared to the DOX treatment alone (Figure 18).

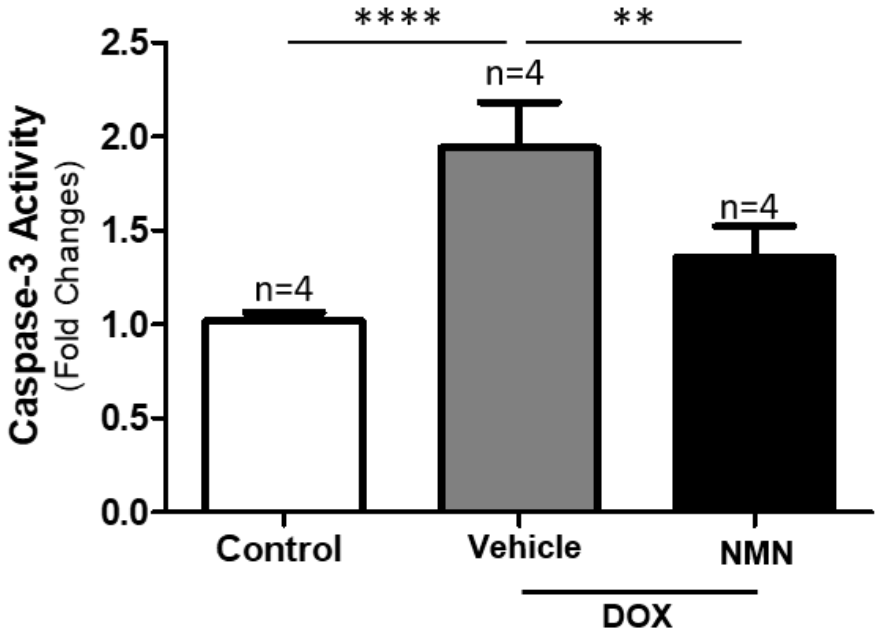

Figure 18: Effect of NMN on caspase-3 activity in H9c2 cells.

H9c2 cells pre-incubated with vehicle or 500 μM of NMN for 18 hours, then 1 μM of DOX for 24 hours in culture media. Caspase-3 activity was determined. Data are provided as means ± SD. A one-way ANOVA analysis followed by the Bonferroni test was performed. A statistical significance was defined by **p-value ≤0.01 and ****p-value ≤ 0.0001.

3.8 NMN abrogates DOX-induced loss of H9c2 cell viability

I measured the cell viability using the calcein AM to determine if NMN can block the loss of cell viability caused by DOX. I seeded H9c2 cells in a 96-well plate at a seeding density of $2.0x10^3$ cells per well. Then, I pre-incubated cells with either vehicle or NMN for 18 hours, then treated cells with DOX for 24 hours in culture media. The result revealed that pre-incubaton with 500 μM of NMN abrogated H9c2 cell viability by about 10% compared to the DOX treated group (Figure 19).

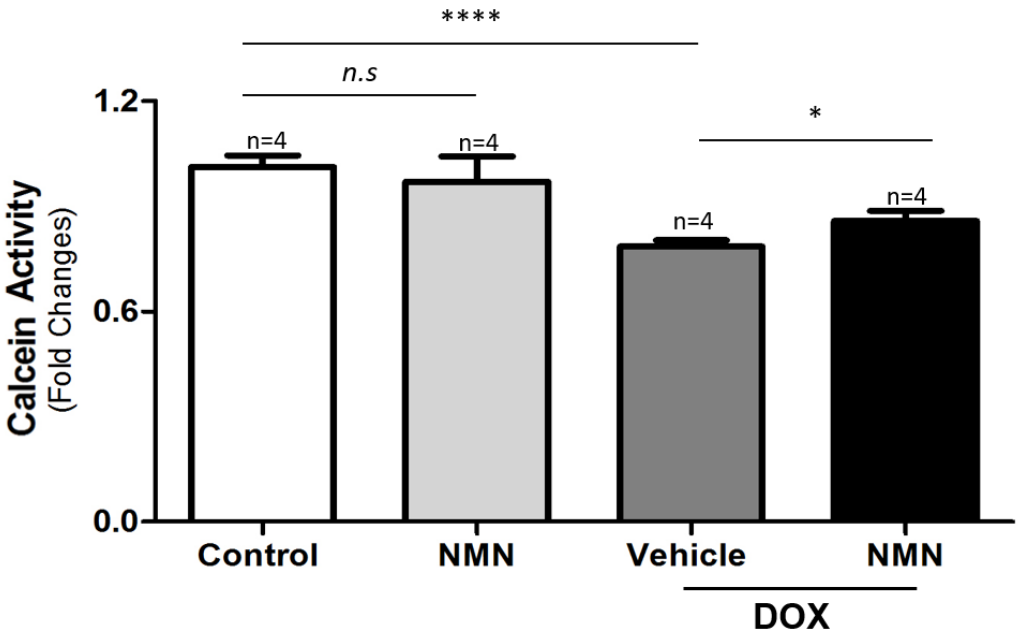

Figure 19: Effect of NMN on DOX-induced loss of H9c2 cell viability.

H9c2 cells pre-incubated either with vehicle or 500 μM of NMN for 18 hours, then 1 μM of DOX for 24 hours in culture media. Cell viability was measured using 1 μM of calcein AM. Data are provided as means ± SD. A one-way ANOVA analysis followed by the Bonferroni test was performed. A statistical significance was defined by *p-value ≤ 0.05, ****p-value ≤ 0.0001, *n.s*=not significant.

3.9 NAD^+ free acid abrogates DOX-induced death in H9c2 cells

I have shown that DOX decreases NAD^+ concentration and pre-incubated cells with NMN boosted NAD^+ in cells (Figure 14). The purpose of this experiment is to determine whether NAD^+ free acid can reduce DOX-induced loss of H9c2 cell viability. I seeded H9c2 cells in a 96-well plate at a seeding density of $2.0x10^3$ cells per well. Cells were treated either with vehicle or NAD^+ free acid for 1 hour, then DOX for 24 hours. When H9c2 cells were pre-incubated with NAD^+ free acid, there was about 10% higher cell viability compared to the DOX treated group (Figure 20).

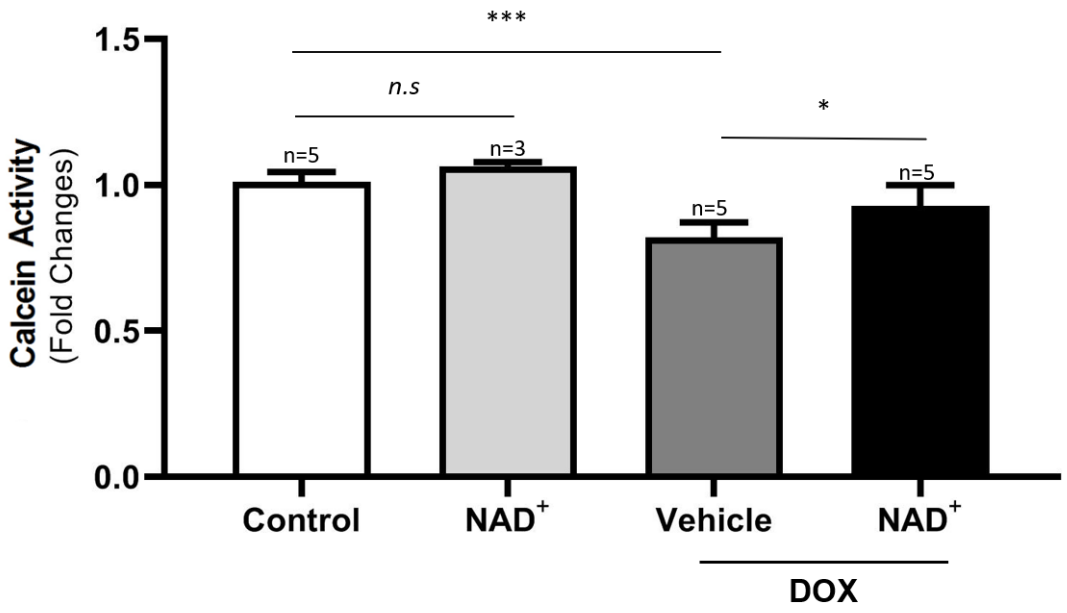

Figure 20: Effect of NAD^+ free acid on DOX-induced cell death in H9c2 cells.
H9c2 cells pre-incubated with either vehicle or 500 μM of NAD^+ for 1 hour, then 1 μM of DOX for 24 hours in culture media. Cell viability was measured using 1 μM of calcein AM. Data are provided as means ± SD. A one-way ANOVA analysis followed by the Bonferroni test was performed. A statistical significance was defined by *p-value ≤ 0.05, ***p-value ≤ 0.001, and *n.s*=not significant.

3.10 NAD^+ free acid decreases caspase-3 activity in H9c2 cells treated with DOX

Since the cell viability assay suggests that NAD^+ free acid provided protection against DOX, I wanted to assess caspase-3 activity. I seeded H9c2 cells in a 24-well plate at a seeding density of $2.0x10^4$ cells per well. Cells were treated either with vehicle or NAD^+ free acid for 1 hour, then DOX for 24 hours. The results showed that cells pre-treated with 500 μM of NAD^+ free acid had about 50% lower caspase-3 activity in comparison to the DOX treated group (Figure 21).

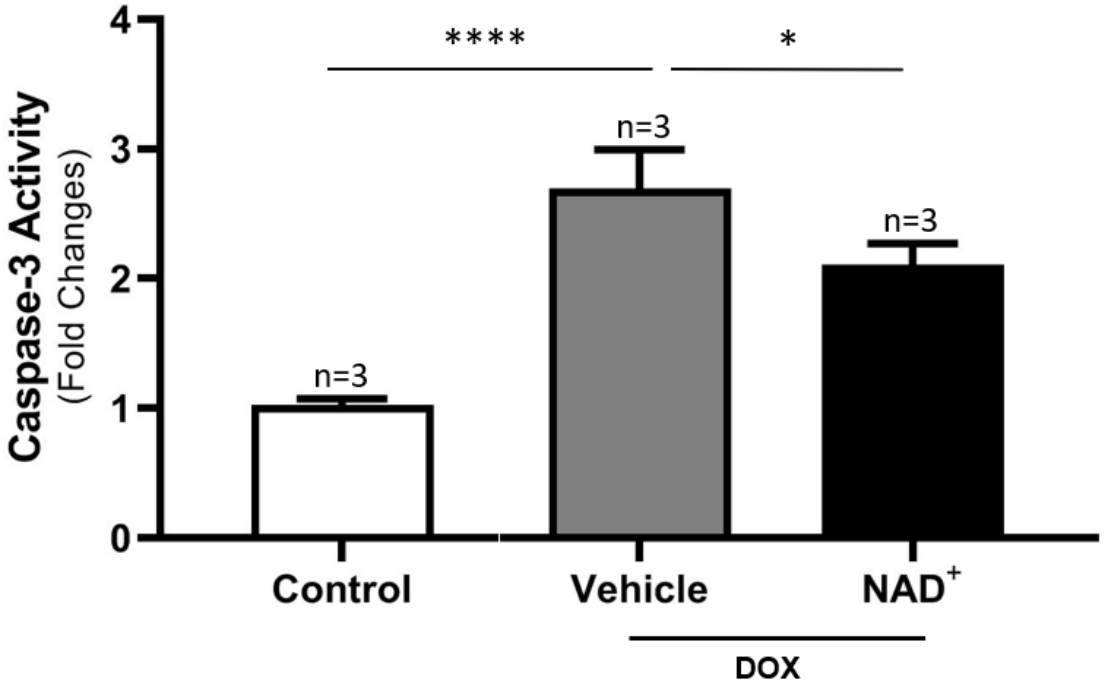

Figure 21: Effect of NAD^+ free acid on caspase-3 activity in H9c2 cells treated with DOX.

H9c2 cells pre-incubated with either vehicle or 500 μM of NAD^+ for 1 hour, then 1 μM of DOX for 24 hours in culture media. Caspase-3 activity was determined. Data are provided as means ± SD. A one-way ANOVA analysis followed by the Bonferroni test was performed. A statistical significance was defined by *p-value ≤ 0.05 and ****p-value ≤ 0.0001.

3.11 Administration of NMN improves myocardial function in DOX-injected mice

To investigate the effect of NMN using *in vivo* methods, I conducted an acute DOX study in mice. Based on a previous study conducted in our laboratory (54), I used a single dose of 500 mg/kg for NMN and 20 mg/kg for DOX. NMN was given 30 minutes before a DOX injection. Five days after DOX injection, the EF and FS percentage were measured as an indicator of myocardial function by echocardiography (Figure 22).

The mean body weight, heart weight, heart rate, LVIDd, and LVIDs for each group can be seen in Table 7. No death occurred in the experiment, but we were unable to obtain the measurements for a mouse in the NMN and saline group. In the DOX injected mice, the EF was about 45% and FS was 22%, indicative of myocardial dysfunction. Mice pre-treated with NMN before DOX injection attenuated myocardial dysfunction as evidenced by the increase in EF to 70% (Figure 23) and increase to 39% in FS (Figure 24).

Table 7: Echocardiography analysis on adult C57BL/6 male mice injected with either NMN (500 mg/kg) or saline for 30 minutes, then a DOX (20 mg/kg) or saline injection.

Treatment Group	N	BW (g)	HW (mg)	HR (beats/min)	LVIDd (mm)	LVIDs (mm)
Vehicle+Saline	5	21.80± 1.94	0.13±0.03	414±69	4.09±0.47	2.34±0.26
NMN+Saline	4	22.77±2.38	0.15±0.04	538±54	4.05±0.51	2.18±0.34
Vehicle+DOX	5	23.31±2.68	0.14±0.04	445±44	4.32±0.60	3.35±0.55
NMN+DOX	5	25.36±1.55	0.12±0.03	470±74	3.95±0.19	2.42±0.19

Data provided as mean ± SD. BW: Body weight, HW: Heart weight, HR: heart rate, LVIDd: left ventricular internal diameter at diastole, LVIDs: left ventricular internal diameter at systole.

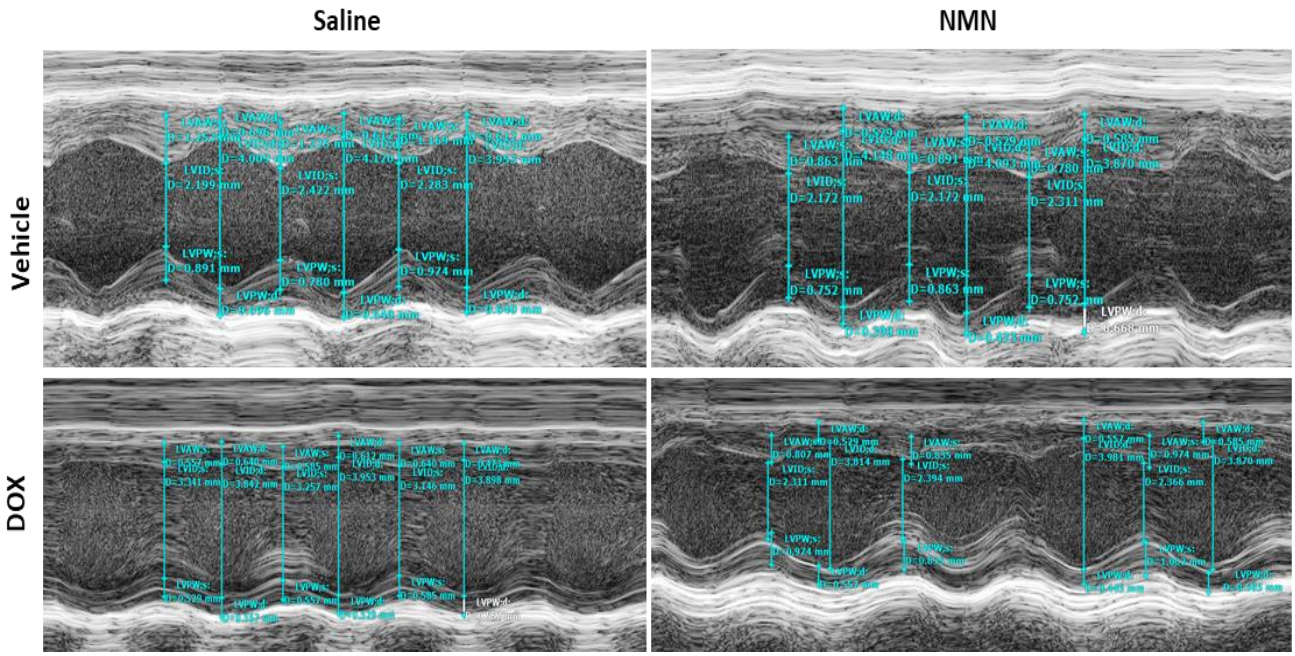

Figure 22: Representative echocardiography image of adult mice in the acute DOX-induced cardiotoxicity study.

Adult C57BL/6 male mice were injected with either NMN (500 mg/kg) or saline for 30 minutes, then received a DOX (20 mg/kg) or saline injection. After 5 days, echocardiography was performed to assess myocardial function.

LVAWd: left ventricular anterior wall at diastole, LVAWs: left ventricular anterior wall at systole, LVIDd: left ventricular internal diameter at diastole, LVIDs: left ventricular internal diameter at systole, LVPWd: left ventricular posterior wall at diastole, LVPWs: left ventricular posterior wall at systole.

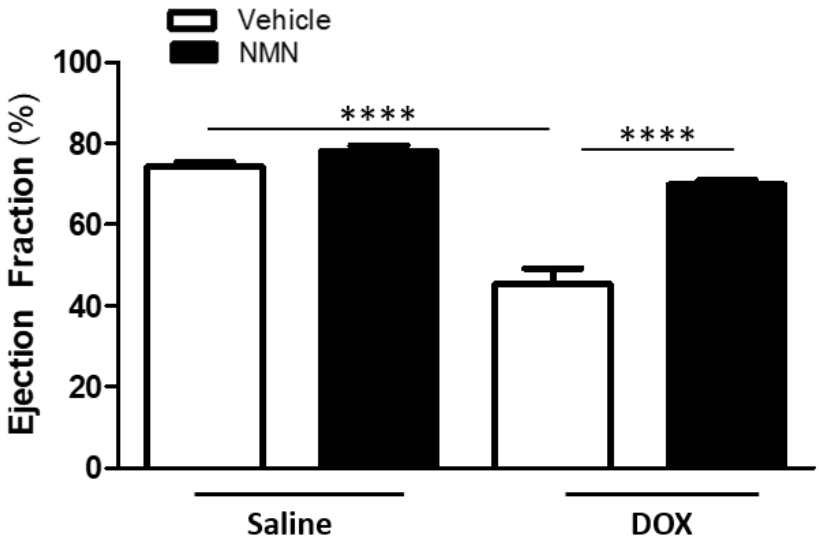

Figure 23: Effect of NMN on ejection fraction in DOX-injected mice.

Adult C57BL/6 male mice were injected with either NMN (500 mg/kg) or saline for 30 minutes, then received a DOX (20 mg/kg) or saline injection. After 5 days, echocardiography was performed to assess myocardial function. Data are provided as means ± SD. A one-way ANOVA analysis followed by the Bonferroni test was performed. A statistical significance was defined by ****p-value ≤ 0.0001.

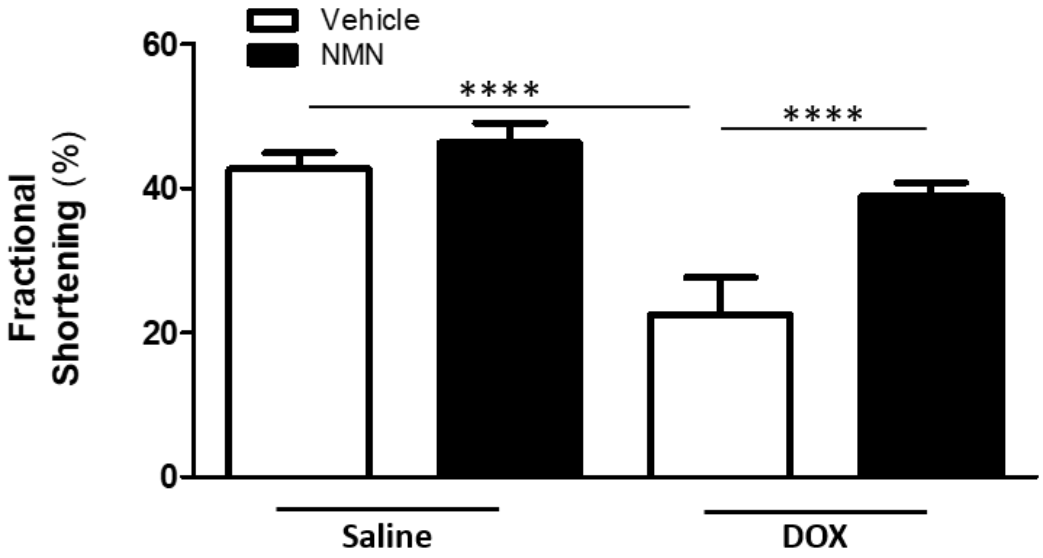

Figure 24: Effect of NMN on fractional shortening in DOX-injected mice.

Adult C57BL/6 male mice were injected with either NMN (500 mg/kg) or saline for 30 minutes, then a received DOX (20 mg/kg) or saline injection. After 5 days, echocardiography was performed to assess myocardial function. Data are provided as means ± SD. Data are provided as means ± SD. A one-way ANOVA analysis followed by the Bonferroni test was performed. A statistical significance was defined by ****p-value ≤ 0.0001.

3.12 NMN reduces cardiac injury in DOX injected mice

The Evans blue dye technique allows for the detection of necrotic cell death. To further assess the *in vivo* effect of NMN, adult mice were treated with NMN (500 mg/kg, i.p.) for 30 minutes or saline and DOX (20 mg/kg, i.p.). After 5 days, the mice were injected with Evans blue (100 mg/kg, i.p.). Four hours later the heart was collected, cryosectioned, and stained with Hoechst 33342 for nuclei (blue colour, Figure 25).

The vehicle saline group did not have any cells stained with Evans blue (red colour, Figure 23). In the NMN pre-incubation group, there were 0.04% of cells stained with Evans blue. The vehicle DOX group had a higher percentage of Evans blue staining at about 1.70% of cells stained. Pre-incubation with NMN decreased cardiac necrosis by lowering Evans blue staining cells to about 0.04% compared to the vehicle DOX group (Figure 26).

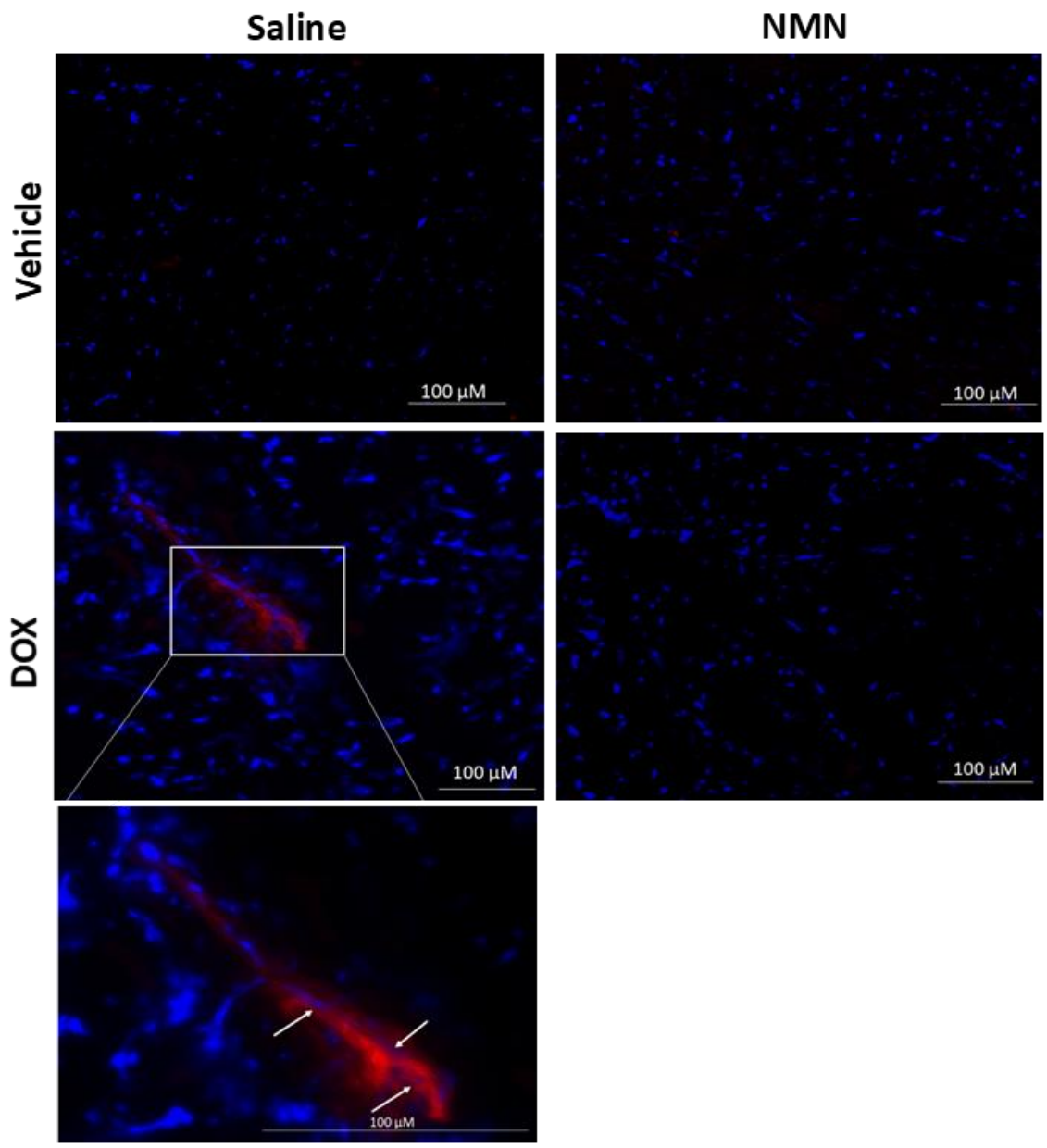

Figure 25: Representative micropictures of Evans Blue staining and nuclear staining.

Evans Blue (100 mg/kg) and Hoechst 33342 (1 mg/mL) staining for cell viability in adult C57BL/6 mice heart tissues 5 days after injection with either NMN (500 mg/kg) or saline for 30 minutes, then a DOX (20 mg/kg) or saline injection. Images were captured on fluorescence microscope at 10x and 40x objective. Arrows are pointing to nuclei within the cardiomyocytes.

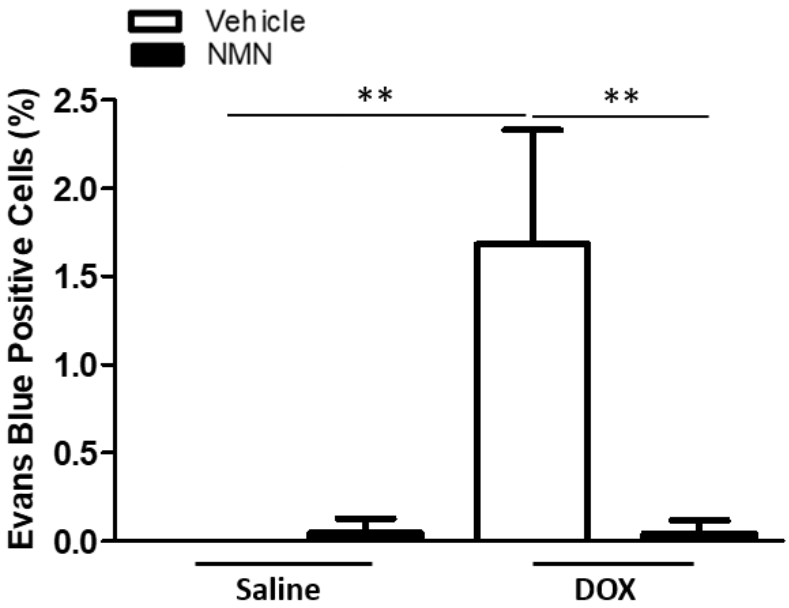

Figure 26: Quantification of Evans Blue positive cells in DOX injected mice.

Evans Blue (100 mg/kg) and Hoechst 33342 (1 mg/mL) staining for cell viability in adult C57BL/6 mice heart tissues 5 days after injection with either NMN (500 mg/kg) or saline for 30 minutes, then a DOX (20 mg/kg) or saline injection. Data are provided as means ± SD. A one-way ANOVA analysis followed by the Bonferroni test was performed. A statistical significance was defined by **p-value ≤ 0.01.

3.13 Inhibition of HAT GCN5 with Butyrolactone 3 does not protect H9c2 cell viability against DOX-induced cardiotoxicity

To determine the role of HAT GCN5, I treated cells with the Butyrolactone 3 inhibitor. I seeded $2.0x10^3$ H9c2 cells per well in a 96-well plate. Cells were either pre-incubated with either vehicle or Butyrolactone 3 for 18 hours, then treated with 1 μM of DOX for 24 hours. I measured the cell viability to help determine cell death using calcein AM. The results showed that the cell viability in the vehicle DOX decreased by about 20% compared to control. Pre-treatment with Butyrolactone 3 at 50 and 100 μM did not affect the cell viability in DOX-treated cells (Figure 27). Therefore, pre-incubating H9c2 cells with Butyrolactone 3 does not abrogate cell death.

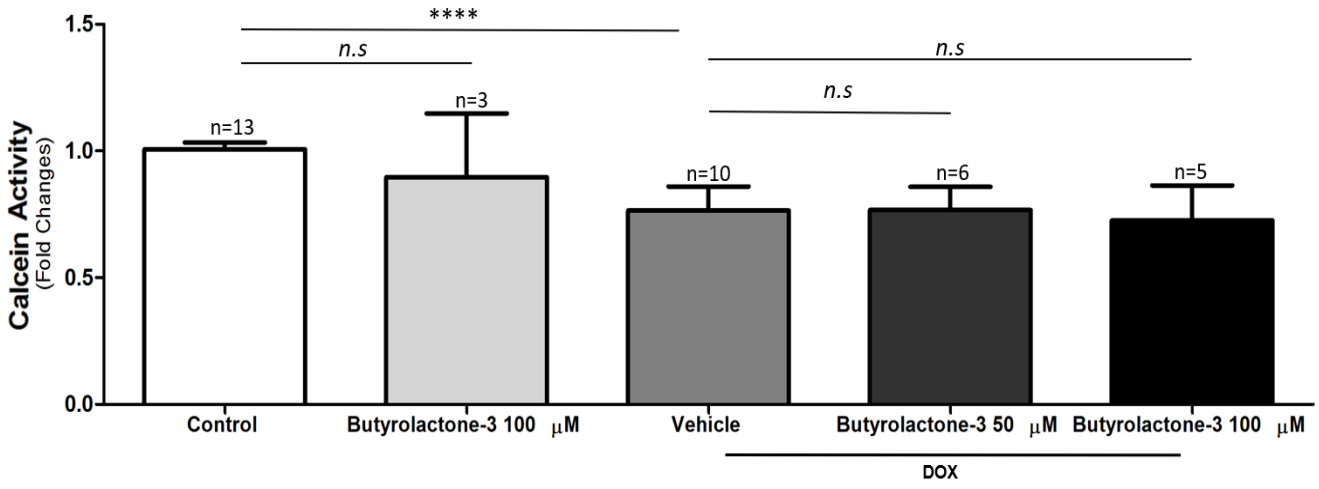

Figure 27: Effect of Butyrolactone 3 on H9c2 cell viability.

H9c2 cells were pre-incubated with either vehicle, 50 μM, or 100 μM of Butyrolactone 3 for 18 hours, then 1 μM of DOX for 24 hours in culture media. Cell viability was measured using 1 μM of calcein AM. Data are provided as means ± SD. A one-way ANOVA analysis followed by the Bonferroni test was performed. A statistical significance was defined by ****p-value ≤ 0.0001 and *n.s*=not significant.

3.14 Inhibition of HAT TIP60 with MG149 does not block the effect of DOX treatment on H9c2 cell viability

I treated cells with the MG149 inhibitor to determine the role of HAT TIP60 in the development of DOX-induced cardiotoxicity. I seeded $2.0x10^3$ H9c2 cells per well into a 96-well plate and either pre-incubated cells with DMSO or the inhibitor for 18 hours, then treated cells with 1 μM of DOX for 24 hours. The results reveal that the percentage of cell viability in the DOX treated and MG149 pre-incubated group were both about 78% (Figure 28). H9c2 cells pre-incubated with MG149 did not block the effect of DOX.

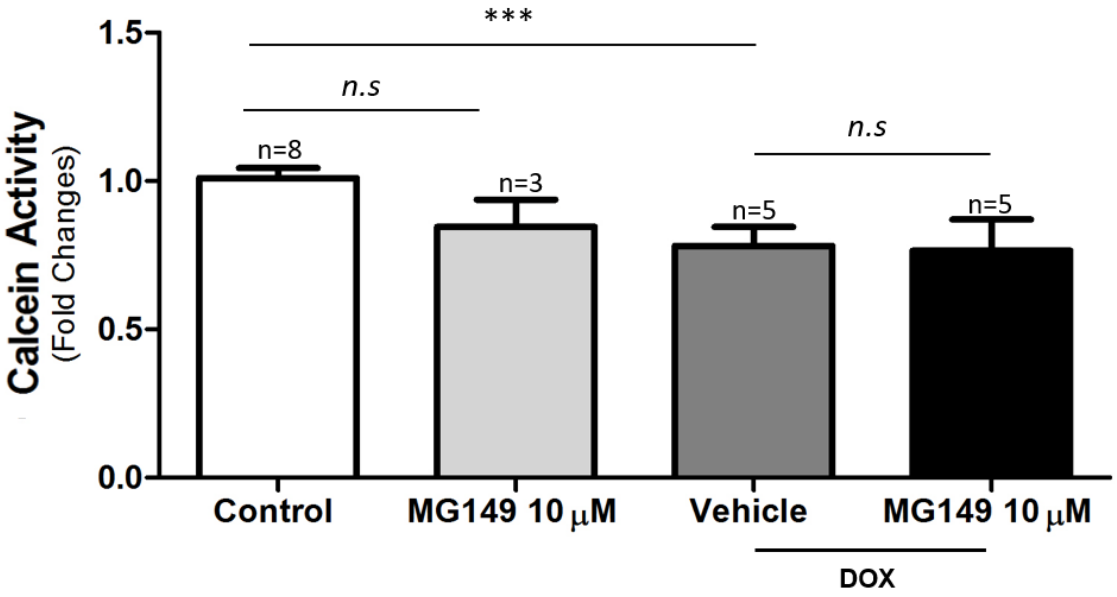

Figure 28: Effect of MG149 on H9c2 cell viability.

H9c2 cells pre-incubated with either vehicle or 10 μM of MG149 for 18 hours, then 1 μM of DOX for 24 hours in culture media. Cell viability was measured using 1 μM of calcein AM. Data are provided as means ± SD. A one-way ANOVA analysis followed by the Bonferroni test was performed. A statistical significance was defined by ***p-value ≤ 0.001 and *n.s*=not significant.

3.15 Inhibition of HAT p300/CBP with C646 does not block DOX's effect on H9c2 cell viability

I determined the role of HAT p300/CBP using the C646 inhibitor. Similar to the previous cell viability experiments, I use the calcein AM assay to determine cell viablilty after treatment with DOX. I seeded $2.0x10^3$ cells per well into a 96-well plate and either pre-incubated cells with either DMSO, 2 μM, 10 μM, or 30 μM of C646 for 18 hours, then 1 μM of DOX for 24 hours in culture media. The results show that the vehicle control group had a 35% decrease in cell viability, indicating lower cell viability than the control. The group pre-treated with 2 μM and 10 μM of C646 had a slight 4% increase in cell viability compared to the vehicle DOX group. Also, the group treated with 30 μM of C646 has the same cell viability percentage as the vehicle DOX treated group (Figure 29). This suggests that C646, an inhibitor of p300 may not be able to prevent DOX-induced cardiotoxicity.

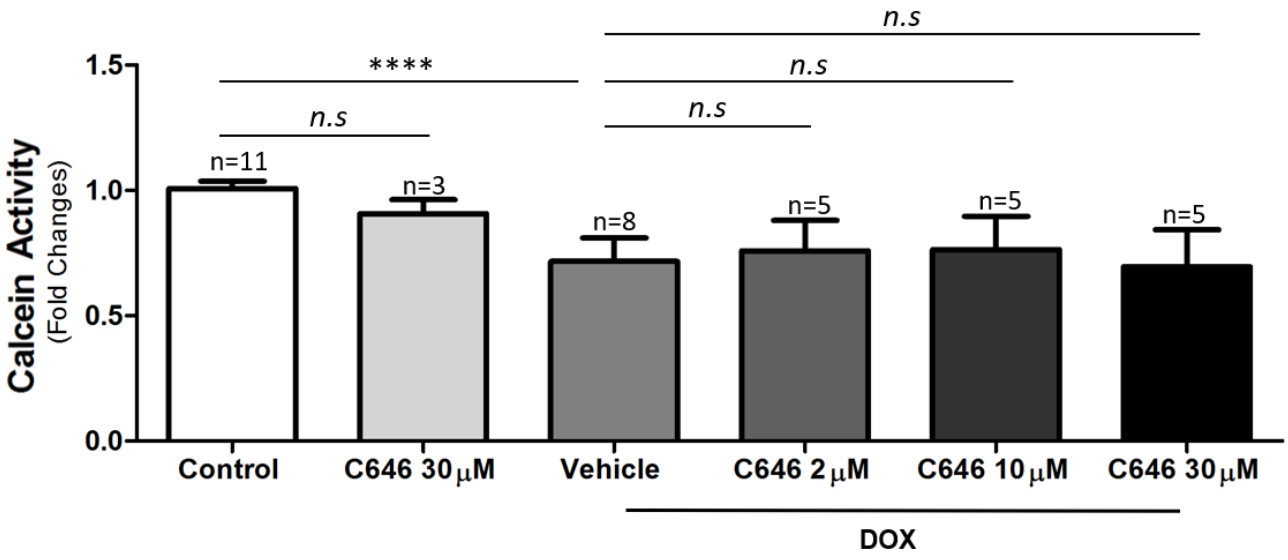

Figure 29: Effect of C646 on H9c2 cell viability.

H9c2 cells pre-incubated with either vehicle, 2 μM, 10 μM, or 30 μM of C646 for 18 hours, then 1 μM of DOX for 24 hours in culture media. Cell viability was measured using 1 μM of calcein AM. Data are provided as means ± SD. A one-way ANOVA analysis followed by the Bonferroni test was performed. A statistical significance was defined by ****p-value ≤ 0.0001 and *n.s*=not significant.

3.16 Inhibition of HAT p300 with HAT inhibitor II does not block DOX effect on H9c2 cell viability

To identify the role of HAT p300, I used the HAT inhibitor II. I used calcein AM to determine the effect of HAT inhibitor II on H9c2 cell viability. I seeded $2.0x10^3$ cells per well into a 96-well plate and either pre-incubated cells with either DMSO or the inhibitor for 18 hours, then 1 μM of DOX for 24 hours. The findings show that there was no difference in H9c2 cell viability when cells were treated with HAT inhibitor II at 5 μM or 10 μM. The vehicle DOX group had a 30% decrease in cell viability compared to the control. The pre-incubated HAT inhibitor II group at 5 μM had an increase in cell viability by 3% compared to the vehicle DOX group. Also, the pre-incubated HAT inhibitor II group at 10 μM had the same cell viability compared to the vehicle DOX group (Figure 30).

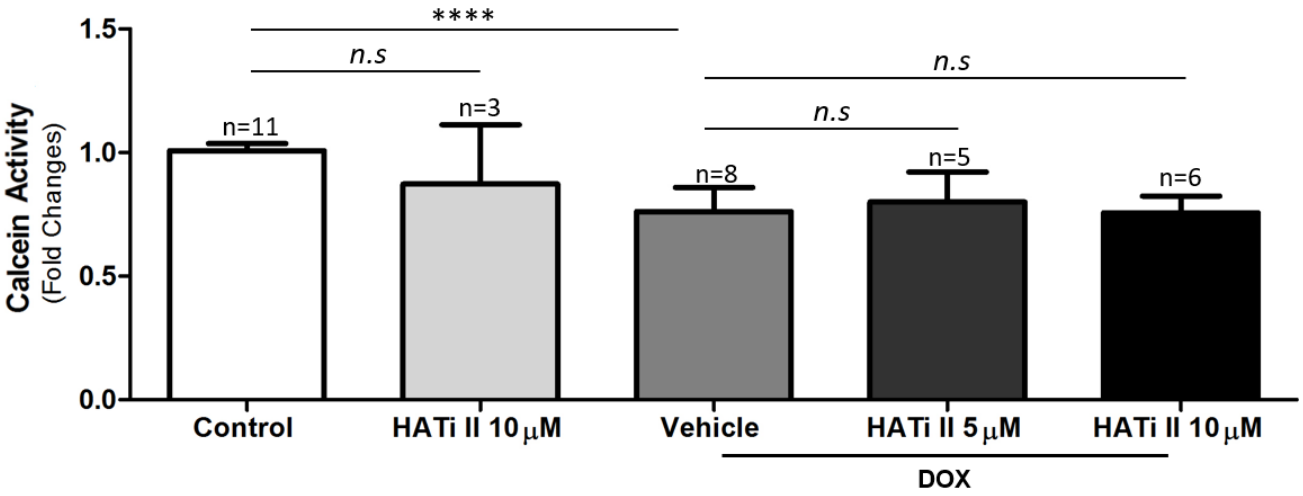

Figure 30: Effect of HAT inhibitor II on H9c2 cell viability.

H9c2 cells pre-incubated with either DMSO, 5 μM, or 10 μM of HAT inhibitor II for 18 hours, then 1 μM of DOX for 24 hours in culture media. Cell viability was measured using 1 μM of calcein AM. Data are provided as means ± SD. A one-way ANOVA analysis followed by the Bonferroni test was performed. A statistical significance was defined by ****p-value ≤ 0.0001 and *n.s*=not significant.

Chapter 4

4 Discussion, Limitations, and Future Directions

4.1 Discussion

4.1.1 DOX induces damage in a dose-dependent manner

DOX induced damage in H9c2 cells in a dose-dependent as revealed by the LDH release (Figure 12), caspase-3 activity (Figure 13), and calcein AM (Figure 14) experiments from 0, 1, 2, and 5 μM of DOX. Our findings are consistent with previously published papers showing DOX induces damage in a dose-dependent manner *in vitro* (86–88). Apoptotic cell death in H9c2 cells was observed to be time and dose-dependent confirming the caspase-3 activity findings in this study (99). Necrosis cell death measured by LDH release shows dose-dependent damage at 24 hours (100).

Further increasing DOX dose above 5 μM decreased H9c2 cell viability in a dose-dependent response manner (101). Thus, we chose to limit our study to 5 μM of DOX. To address why the concentration at 50% of cell viability loss varies across the different studies, it may be a difference in passage number that affects increases cellular sensitivity to stress conditions (102). There is a consistent trend from previous studies and this study that DOX elicits damage in a dose-dependent manner.

4.1.2 Increasing NAD^+ concentration prevents DOX damage in H9c2 cells

DOX reduces NAD^+ concentration (Figure 15) and pre-treating with NMN does promote NAD^+ in H9c2 cells (Figure 16). Pre-treating H9c2 cells with NMN before DOX treatment reduced LDH release (Figure 17) and lower caspase-3 activity (Figure 18). Also, cell viability increased with pre-treatment of NMN compared to the DOX only group (Figure 19). We have shown that NMN can attenuate DOX-induced cardiotoxicity by increasing NAD^+ concentration in H9c2 cells. Our study reveals novel *in vitro* findings that NMN protects against DOX-induced cardiotoxicity through increasing NAD^+ concentration to prevent cell death. Furthermore, pre-incubating H9c2 cells with

NAD^+ free acid for 1 hour resulted in higher cell viability (Figure 20) and decreased caspase-3 activity (Figure 21). This finding is consistent with previous research that exogenous NAD^+ increased intracellular NAD^+ concentration in H9c2 cells (103).

The downstream molecular mechanisms following NAD^+ was not examined in this study. Previous research shows that EX-527 attenuated the protective effect of NR, which suggests that NR acts through the NAD^+/SIRT1 pathway (54). We predict that NMN could function through the same pathway to provide protection. SIRT1 is involved in inducing autophagy to protect cardiomyocytes from stressors (104). SIRT1 may directly facilitate autophagic flux by preventing acetylation on Vacuolar ATPase and maintaining the acidic lysosomal environment to allow for degradation of accumulated cargo (30). Further investigation into the molecular mechanisms including the relationship between SIRT1 and Vacuolar ATPase would be important to understanding DOX-induced cardiotoxicity's mechanism.

4.1.3 NMN protects mice hearts against DOX

EF% is the percentage of volumetric blood that is being pumped out of the heart per cardiac cycle. A decline in EF% indicates that the heart is not effectively pumping as much blood volume out, thus there is blood remaining in the ventricle. FS% is the percentage of change in the diameter of the ventricle after a cardiac cycle. Similarly, a decrease in FS% suggests a decrease in cardiac function. We found that 5 days after a DOX injection, mice pre-treated with NMN had higher EF% (Figure 23) and FS% (Figure 24) compared to the vehicle treated group, which indicates improved myocardial function.

We can confirm that the Evans Blue dye stained for cardiomyocytes as the cell has an elongated rod shape and contains multiple nuclei (Figure 25) (105,106). Evans Blue staining showed that mice injected with NMN before DOX had fewer positive cells stained compared to DOX only group (Figure 26). This indicates that there is reduced cardiac injury. It has been shown that DOX induced necrosis on cardiomyocytes and NR

was able to inhibit DOX's effect using the Evans Blue technique (54). No published studies have examined NMN's effect on DOX treated mice using Evans Blue staining.

The results from this study are consistent with a published article that shows NMN converts into NAD^+ to preserve cardiac function (58). NMN supplementation prevented cardiomyopathy by increasing heart tissue NAD^+ concentration in DOX treated mice (58), similar to our *in vitro* results (Figure 14). Our *in vivo* finding is the first to show that NMN can protect mouse hearts from an acute DOX-induced cardiotoxicity study. We have provided novel data from the Evans Blue data to further support NMN protective effects. Therefore, boosting NAD^+ with NMN protects against DOX-induced cardiotoxicity in the H9c2 cell line and attenuates myocardial dysfunction in DOX-injected adult mice.

While NR has previously shown cardioprotective effects, NMN contains several potential advantages over NR. A newly discovered NMN transporter has shown that NMN can directly enter the cell (52). Direct entry into the cell makes NMN conversion into NAD^+ more effective since it does not dependent on the rate-limiting activity of NRK1/2. Furthermore, NR is more unstable and degrades into NAM in murine plasma compared to NMN (50). NMN can be rapidly absorbed into the blood circulation from the gut within 3 minutes, then into tissues within 15 minutes (107,108). Therefore, NMN has several advantages over NR and is a promising compound for future research.

4.1.4 Selective HAT inhibitors have no effect on H9c2 cells treated with DOX

We selected the HAT inhibitors in this study based on 3 criteria including specificity, availability, and cost of HAT inhibitors. The first criterion is the specificity of the HAT inhibitor. We choose HAT inhibitors that would inhibit specific HAT family members since we would be able to eliminate or attribute the effect to a specific member. The second criterion is the availability of the HAT inhibitors, where we selected HAT inhibitors that were readily available from a pharmaceutical company. Lastly, the final criterion is the cost of the HAT inhibitors, and this criterion helps to ensure that the

project was feasible. Based on these criteria, we selected Butyrolactone 3, MG149, C646, and HAT inhibitor II.

In this study, we found there was no effect on H9c2 cell viability when treated with the various HAT inhibitors. Butyrolactone 3 inhibits HAT GNC5 and there was no effect on H9c2 cells when pre-treated with the inhibitor for 18 hours before DOX treatment (Figure 27). Currently, no studies have examined the effect of Butyrolactone 3 in DOX-induced cardiotoxicity. Our finding provides novel insight into the effect of Butyrolactone 3 on H9c2 cell viability treated with DOX.

Similarly, when H9c2 cells were treated with MG149, which inhibits HAT TIP60, we showed that MG149 at 10 μM did not affect cell viability (Figure 28). A recently published article revealed that hyperacetylation of GATA4, a member of the GATA transcription factor family protected against DOX (109). While the hypoacetylation caused by administering MG149 at 20 μM resulted in a loss of its protective effect (109). DOX treatment impairs the SIRT6-TIP60-GATA4 trimeric complex which blocks GATA4 acetylation leading to cardiomyocyte apoptosis (109). These findings contradict our proposed model, as the regulation between SIRT6 and TIP60 function together to prevent DOX-induced cardiotoxicity. One potential reason as to why our results are inconsistent with the published article maybe because we used a lower dosage. Nevertheless, our finding provides information into the effect of MG149 on H9c2 cells treated with DOX.

There was no effect on H9c2 cell viability when pre-treated with HAT p300/CBP inhibitor C646 at 2, 10, and 30 μM compared to DOX treatment alone (Figure 29). A study that revealed inhibition of p53 acetylation with C646 prevented DOX-induced cardiotoxicity in normal bone marrow cells with maintaining DOX's anti-cancer efficacy (74). C646 prevented DOX-induced toxicity by inhibiting p53 activity, a substrate to p300 (74). We have provided new evidence to show that C646 has no effect on H9c2 cell viability treated with DOX.

We found that pre-treating H9c2 cells with HAT inhibitor II at 5 and 10 μM, which inhibits p300 did not have an effect (Figure 30). To date, there are no studies examining HAT inhibitor II in the development of DOX-induced cardiotoxicity. Therefore, our finding provides novel insight into the effect of HAT inhibitor II on cells treated with DOX.

In summary, pre-treatment of HAT inhibitors has no effect on H9c2 cell viability treated with DOX. We have showcased new insights into the effects of various HAT inhibitors on H9c2 cell viability treated with DOX. Based on our findings, it suggests that HATs GCN5, TIP60, and p300/CBP does not play a role in DOX-induced cardiotoxicity. Further studies to determine whether other HAT family members are involved is required to fully understand the role of HAT in DOX-induced cardiotoxicity.

4.2 Limitations

There are several limitations to the NMN research study that requires further investigation. We conducted an acute DOX-induced cardiotoxicity model with a single DOX injection for 5 days. The findings from our acute DOX-induced cardiotoxicity study may not be clinically relevant or be generalized to chronic DOX-induced cardiotoxicity, it does provide useful insights potential therapeutics for DOX-induced cardiotoxicity. Also, the research project does not examine the effect of NMN on DOX's anti-cancer effect. The focus of our research project was to determine and understand NMN's protective properties against DOX. We did not examine whether pre-treating cells with NMN affected DOX's ability to stop cancer cell proliferation. However, it has been shown that NAD^+ prevents cancer cell metabolism and provides an anti-tumor effect in cancers (110,111).

There are several limitations to the HAT study as well. First, the selected HAT inhibitors that were used in this study did not protect against DOX in H9c2 cells. There are multiple different HAT inhibitors and the chosen inhibitors in this study including HAT inhibitor II, MG149, Butyrolactone 3, and C646, were based on availability on the market, cost, and selective inhibition on HAT family member. One reason why the HAT inhibitor

shows no effect may be because the inhibitor functions to inhibit a specific HAT family member, while other HAT members may be able to compensate for the loss of activity. For example, Butyrolactone 3 inhibits GCN5 activity, however with the reduced activity of GCN5, perhaps PCAF increases its activity to compensate for the loss (112). Therefore, the global activity of HAT remains the same and results in DOX-induced cardiotoxicity.

4.3 Future Directions

To address the NMN limitations, a future direction is to conduct a study to determine if the protective effects of NMN are consistent in a chronic model of DOX-induced cardiotoxicity in adult mice as well, a more clinically relevant model. Being able to replicate the findings in a chronic mice model would further confirm NMN protective effects against DOX in an acute and chronic mice model. Another future direction would be to examine whether NMN impacts DOX's anti-cancer activity. DOX's functions through a multiple mechanism of action and whether NMN interferes remains to be determined. NR was found to prevent tumour formation (113), so NMN could have a similar effect on tumours growth which would further support its merits for clinical use.

Other HAT inhibitors could be effective in preventing DOX-induced cardiotoxicity. Another future direction would be to use a Pan-HAT inhibitor, which will inhibit the activity of multiple HAT family members. This will help to further help understand the role of HAT in the development of DOX-induced cardiotoxicity by inhibiting various HAT family members at once. There is a pan-HAT inhibitor called PU139, which blocks GCN5, PCAF, CBP, and p300 (114). Researchers found that when PU139 was combined with DOX, there was a synergistic effect on blocking the growth of neuroblastoma cells (114). With limited research on the effect of PU139, it is difficult to determine the effect on non-cancerous cells. We predict that a pan-HAT inhibitor can lower acetylation levels in cardiomyocytes to protect against DOX.

4.4 Project Significance

Intense efforts should be taken to establish preventive options against DOX-induced cardiotoxicity as the number of cancer patients will rise. Our research contributes to discovering potential preventive therapeutic options for patients suffering from DOX-induced cardiotoxicity. NMN may be a potential preventive option for patients experiencing DOX-induced cardiotoxicity. Thus, this study lays an important foundation for future clinical trials using NMN to prevent DOX-induced cardiotoxicity in patients receiving anthracycline chemotherapy.

Furthermore, the results from the HAT inhibitor study suggest that specific HAT family members may not be involved in DOX-induced cardiotoxicity. With limited studies examining HAT in DOX-induced cardiotoxicity, this study contributes to advancing scientific literature and identifying the potential roles of HATs.

4.5 Concluding Remarks

The main findings in this study reveal that pre-treatment of NMN prevented DOX damage by increasing NAD^+ concentration and that NMN is an effective approach to reduce DOX-induced cardiotoxicity. Although the molecular mechanism is not fully elucidated, this study shows that NAD^+ plays an important role in preventing DOX's damage. Since NMN is a health supplement, our findings can be conveniently translated into clinical patients in the future.

HAT inhibitors Butyrolactone 3, MG149, C646, and HAT inhibitor II has no effect on H9c2 cells treated with DOX. Further research into HATs and HDACs are required to understand its' effect in the development of DOX-induced cardiotoxicity.

References

1. WHO Key statistics. WHO. Available from: https://www.who.int/cancer/resources/keyfacts/en/

2. McGowan JV, Chung R, Maulik A, Piotrowska I, Walker JM, Yellon DM. Anthracycline Chemotherapy and Cardiotoxicity. Cardiovascular Drugs and Therapy. 2017 Feb;31(1):63–75.

3. Xing M, Yan F, Yu S, Shen P. Efficacy and Cardiotoxicity of Liposomal Doxorubicin-Based Chemotherapy in Advanced Breast Cancer: A Meta-Analysis of Ten Randomized Controlled Trials. PLOS ONE. 2015 Jul 23;10(7):e0133569.

4. Cassinelli G. The Roots of Modern Oncology: From Discovery of New Antitumor Anthracyclines to their Clinical Use. Tumori. 2016 May 1;102(3):226–35.

5. Tacar O, Sriamornsak P, Dass CR. Doxorubicin: an update on anticancer molecular action, toxicity and novel drug delivery systems: Doxorubicin cell and molecular biological activity. Journal of Pharmacy and Pharmacology. 2013 Feb;65(2):157–70.

6. Chemical Structure of Doxorubicin. 2007. Available from: https://commons.wikimedia.org/wiki/File:Doxorubicin.svg

7. Structure of Daunorubicin. 2013. Available from: https://commons.wikimedia.org/wiki/File:Daunorubicin2DACS.svg

8. Adriamycin (DOXOrubicin HCl) for Injection. Bedford, OH: Ben Venue Laboratorie; 2002. Available from: https://www.accessdata.fda.gov/drugsatfda_docs/label/2012/062921s022lbl.pdf

9. Bodley A, Liu LF, Israel M, Seshadri R, Koseki Y, Giuliani FC, et al. DNA Topoisomerase II-mediated Interaction of Doxorubicin and Daunorubicin Congeners with DNA. Cancer Res. 1989 Nov 1;49(21):5969–78.

10. Doroshow JH. Effect of anthracycline antibiotics on oxygen radical formation in rat heart. Cancer research. 1983 Feb 1;43(2):460-72.

11. Doroshow JH. Role of hydrogen peroxide and hydroxyl radical formation in the killing of Ehrlich tumor cells by anticancer quinones. PNAS. 1986 Jun 1;83(12):4514–8.

12. Chatterjee K, Zhang J, Honbo N, Karliner JS. Doxorubicin Cardiomyopathy. Cardiology. 2010;115(2):155–62.

13. Hershman DL, McBride RB, Eisenberger A, Tsai WY, Grann VR, Jacobson JS. Doxorubicin, Cardiac Risk Factors, and Cardiac Toxicity in Elderly Patients With Diffuse B-Cell Non-Hodgkin's Lymphoma. Journal of Clinical Oncology.

14. Swain SM, Whaley FS, Ewer MS. Congestive heart failure in patients treated with doxorubicin: a retrospective analysis of three trials. Cancer: Interdisciplinary International Journal of the American Cancer Society. 2003 Jun 1;97(11):2869-79.

15. Green DM, Grigoriev YA, Nan B, Takashima JR, Norkool PA, D'Angio GJ, et al. Congestive Heart Failure After Treatment for Wilms' Tumor: A Report From the National Wilms' Tumor Study Group. JCO. 2001 Apr 1;19(7):1926–34.

16. Lipshultz SE, Lipsitz SR, Mone SM, Goorin AM, Sallan SE, Sanders SP, et al. Female Sex and Higher Drug Dose as Risk Factors for Late Cardiotoxic Effects of Doxorubicin Therapy for Childhood Cancer. New England Journal of Medicine. 1995 Jun 29;332(26):1738–44.

17. Vachhani P, Shin S, Baron J, Thompson JE, Wetzler M, Griffiths EA, et al. Dexrazoxane for cardioprotection in older adults with acute myeloid leukemia. Leukemia Research Reports. 2017 Jan 1;7:36–9.

18. Langer S. Dexrazoxane for the treatment of chemotherapy-related side effects. Cancer Management and Research. 2014 Sep;357.

19. Shaikh F, Dupuis LL, Alexander S, Gupta A, Mertens L, Nathan PC. Cardioprotection and Second Malignant Neoplasms Associated With Dexrazoxane in Children Receiving Anthracycline Chemotherapy: A Systematic Review and Meta-Analysis. J Natl Cancer Inst. 2016 Apr;108(4).

20. Gupta V, Singh SK, Agrawal V, Singh TB. Role of ACE inhibitors in anthracycline-induced cardiotoxicity: A randomized, double-blind, placebo-controlled trial. Pediatric Blood & Cancer. 2018;65(11):e27308.

21. Abuosa AM, Elshiekh AH, Qureshi K, Abrar MB, Kholeif MA, Kinsara AJ, et al. Prophylactic use of carvedilol to prevent ventricular dysfunction in patients with cancer treated with doxorubicin. Indian Heart Journal. 2018 Dec 1;70:S96–100.

22. Seicean S, Seicean A, Plana JC, Budd GT, Marwick TH. Effect of Statin Therapy on the Risk for Incident Heart Failure in Patients With Breast Cancer Receiving Anthracycline Chemotherapy: An Observational Clinical Cohort Study. Journal of the American College of Cardiology. 2012 Dec 11;60(23):2384–90.

23. Hicks BM, Filion KB, Yin H, Sakr L, Udell JA, Azoulay L. Angiotensin converting enzyme inhibitors and risk of lung cancer: population based cohort study. BMJ. 2018 Oct 24;363.

24. Jansen L, Weberpals J, Kuiper JG, Vissers PAJ, Wolkewitz M, Hoffmeister M, et al. Pre- and post-diagnostic beta-blocker use and prognosis after colorectal cancer:

Results from a population-based study. International Journal of Cancer. 2017;141(1):62–71.

25. Cappetta D, De Angelis A, Sapio L, Prezioso L, Illiano M, Quaini F, et al. Oxidative Stress and Cellular Response to Doxorubicin: A Common Factor in the Complex Milieu of Anthracycline Cardiotoxicity. Oxid Med Cell Longev. 2017.

26. Pecoraro M, Rodríguez-Sinovas A, Marzocco S, Ciccarelli M, Iaccarino G, Pinto A, et al. Cardiotoxic Effects of Short-Term Doxorubicin Administration: Involvement of Connexin 43 in Calcium Impairment. Int J Mol Sci. 2017;18(10).

27. He H, Luo Y, Qiao Y, Zhang Z, Yin D, Yao J, et al. Curcumin attenuates doxorubicin-induced cardiotoxicity via suppressing oxidative stress and preventing mitochondrial dysfunction mediated by 14-3-3γ. Food Funct. 2018 Aug 15;9(8):4404–18.

28. Rharass T, Gbankoto A, Canal C, Kurşunluoğlu G, Bijoux A, Panáková D, et al. Oxidative stress does not play a primary role in the toxicity induced with clinical doses of doxorubicin in myocardial H9c2 cells. Mol Cell Biochem. 2016 Feb;413(1–2):199–215.

29. Yoshii SR, Mizushima N. Monitoring and measuring autophagy. International journal of molecular sciences. 2017 Sep;18(9):1865.

30. Li DL, Wang ZV, Ding G, Tan W, Luo X, Criollo A, Xie M, Jiang N, May H, Kyrychenko V, Schneider JW. Doxorubicin blocks cardiomyocyte autophagic flux by inhibiting lysosome acidification. Circulation. 2016 Apr 26;133(17):1668-87.

31. Zhang Y-Y, Meng C, Zhang X-M, Yuan C-H, Wen M-D, Chen Z, et al. Ophiopogonin D Attenuates Doxorubicin-Induced Autophagic Cell Death by Relieving Mitochondrial Damage In Vitro and In Vivo. J Pharmacol Exp Ther. 2015 Jan 1;352(1):166–74.

32. Koleini N, Kardami E. Autophagy and mitophagy in the context of doxorubicin-induced cardiotoxicity. Oncotarget. 2017 Jul 11;8(28):46663.

33. Bartlett JJ, Trivedi PC, Pulinilkunnil T. Autophagic dysregulation in doxorubicin cardiomyopathy. Journal of Molecular and Cellular Cardiology. 2017 Mar;104:1–8.

34. Park J, Choi S, Kim H, Ji S, Jang W, Kim J, et al. Doxorubicin Regulates Autophagy Signals via Accumulation of Cytosolic Ca2+ in Human Cardiac Progenitor Cells. International Journal of Molecular Sciences. 2016 Oct 9;17(10):1680.

35. Xiao W, Wang R-S, Handy DE, Loscalzo J. NAD(H) and NADP(H) Redox Couples and Cellular Energy Metabolism. Antioxidants & Redox Signaling. 2018 Jan 20;28(3):251–72.

36. NEUROtiker. Structure of nicotinamide adenine dinucleotide, oxidized (NAD+). 2007. Available from: https://commons.wikimedia.org/wiki/File:NAD%2B_phys.svg

37. Fricker RA, Green EL, Jenkins SI, Griffin SM. The Influence of Nicotinamide on Health and Disease in the Central Nervous System. International Journal of Tryptophan Research. 2018 Jan;11:117864691877665.

38. MacKay D, Hathcock J, Guarneri E. Niacin: chemical forms, bioavailability, and health effects. Nutr Rev. 2012 Jun 1;70(6):357–66.

39. Martens CR, Denman BA, Mazzo MR, Armstrong ML, Reisdorph N, McQueen MB, et al. Chronic nicotinamide riboside supplementation is well-tolerated and elevates NAD + in healthy middle-aged and older adults. Nature Communications. 2018 Mar 29;9(1):1–11.

40. Pittelli M, Felici R, Pitozzi V, Giovannelli L, Bigagli E, Cialdai F, et al. Pharmacological Effects of Exogenous NAD on Mitochondrial Bioenergetics, DNA Repair, and Apoptosis. Mol Pharmacol. 2011 Dec 1;80(6):1136–46.

41. Aman Y, Qiu Y, Tao J, Fang EF. Therapeutic potential of boosting NAD+ in aging and age-related diseases. Translational Medicine of Aging. 2018 Jan 1;2:30–7.

42. Trammell SA, Weidemann BJ, Chadda A, Yorek MS, Holmes A, Coppey LJ, Obrosov A, Kardon RH, Yorek MA, Brenner C. Nicotinamide riboside opposes type 2 diabetes and neuropathy in mice. Scientific reports. 2016 May 27;6:26933.

43. Biefer HRC, Elkhal A, Cesarovic N, Emmert MY. NAD+ the disregarded molecule in cardiac metabolism. Eur Heart J. 2020 Mar 1;41(9):983–6.

44. Mori V, Amici A, Mazzola F, Di Stefano M, Conforti L, Magni G, et al. Metabolic Profiling of Alternative NAD Biosynthetic Routes in Mouse Tissues. de Crécy-Lagard V, editor. PLoS ONE. 2014 Nov 25;9(11):e113939.

45. Cantó C, Menzies KJ, Auwerx J. NAD+ Metabolism and the Control of Energy Homeostasis: A Balancing Act between Mitochondria and the Nucleus. Cell Metabolism. 2015 Jul;22(1):31–53.

46. Venter G, Oerlemans FTJJ, Willemse M, Wijers M, Fransen JAM, Wieringa B. NAMPT-Mediated Salvage Synthesis of NAD+ Controls Morphofunctional Changes of Macrophages. Dzeja P, editor. PLoS ONE. 2014 May 13;9(5):e97378.

47. Verdin E. NAD+ in aging, metabolism, and neurodegeneration. Science. 2015 Dec 4;350(6265):1208–13.

48. Kane Alice E., Sinclair David A. Sirtuins and NAD+ in the Development and Treatment of Metabolic and Cardiovascular Diseases. Circulation Research. 2018 Sep 14;123(7):868–85.

49. Tempel W, Rabeh WM, Bogan KL, Belenky P, Wojcik M, Seidle HF, et al. Nicotinamide Riboside Kinase Structures Reveal New Pathways to NAD+. PLOS Biology. 2007 Oct 2;5(10):e263.

50. Ratajczak J, Joffraud M, Trammell SA, Ras R, Canela N, Boutant M, Kulkarni SS, Rodrigues M, Redpath P, Migaud ME, Auwerx J. NRK1 controls nicotinamide mononucleotide and nicotinamide riboside metabolism in mammalian cells. Nature communications. 2016 Oct 11;7(1):1-2.

51. Nikiforov A, Dölle C, Niere M, Ziegler M. Pathways and subcellular compartmentation of NAD biosynthesis in human cells from entry of extracellular precursors to mitochondrial NAD generation. Journal of Biological Chemistry. 2011 Jun 17;286(24):21767-78.

52. Grozio A, Mills KF, Yoshino J, Bruzzone S, Sociali G, Tokizane K, et al. Slc12a8 is a nicotinamide mononucleotide transporter. Nature Metabolism. 2019 Jan;1(1):47–57.

53. Diguet N, Trammell SAJ, Tannous C, Deloux R, Piquereau J, Mougenot N, et al. Nicotinamide Riboside Preserves Cardiac Function in a Mouse Model of Dilated Cardiomyopathy. Circulation. 2018 22;137(21):2256–73.

54. Zheng D, Zhang Y, Zheng M, Cao T, Wang G, Zhang L, et al. Nicotinamide riboside promotes autolysosome clearance in preventing doxorubicin-induced cardiotoxicity. Clin Sci (Lond). 2019 Jul 15;133(13):1505–21.

55. Chemical structure of Nicotinamide-beta-riboside. 2014. Available from: https://commons.wikimedia.org/wiki/File:Nicotinamide-beta-riboside.svg

56. Martin AS, Abraham DM, Hershberger KA, Bhatt DP, Mao L, Cui H, Liu J, Liu X, Muehlbauer MJ, Grimsrud PA, Locasale JW. Nicotinamide mononucleotide requires SIRT3 to improve cardiac function and bioenergetics in a Friedreich's ataxia cardiomyopathy model. JCI insight. 2017 Jul 20;2(14).

57. Yamamoto T, Byun J, Zhai P, Ikeda Y, Oka S, Sadoshima J. Nicotinamide Mononucleotide, an Intermediate of NAD+ Synthesis, Protects the Heart from Ischemia and Reperfusion. Hosoda T, editor. PLoS ONE. 2014 Jun 6;9(6):e98972.

58. Li J, Wang P, Long NA, Zhuang J, Springer DA, Zou J, et al. p53 prevents doxorubicin cardiotoxicity independently of its prototypical tumor suppressor activities. Proceedings of the National Academy of Sciences. 2019 Sep 24;116(39):19626–34.

59. Chemical structure of nicotinamide nicotinamide mononucleotide. 2016. Available from: https://commons.wikimedia.org/wiki/File:Nicotinamide_mononucleotide.svg

60. Seto E, Yoshida M. Erasers of Histone Acetylation: The Histone Deacetylase Enzymes. Cold Spring Harbor Perspectives in Biology. 2014 Apr 1;6(4):a018713–a018713.

61. Ververis K, Rodd AL, Tang MM, El-Osta A, Karagiannis TC. Histone deacetylase inhibitors augment doxorubicin-induced DNA damage in cardiomyocytes. Cellular and Molecular Life Sciences. 2011 Dec;68(24):4101–14.

62. Holbert MA, Marmorstein R. Structure and activity of enzymes that remove histone modifications. Current Opinion in Structural Biology. 2005 Dec 1;15(6):673–80.

63. Alexander SP, Fabbro D, Kelly E, Mathie A, Peters JA, Veale EL, Armstrong JF, Faccenda E, Harding SD, Pawson AJ, Sharman JL. The concise guide to pharmacology 2019/20: Enzymes. British Journal of Pharmacology. 2019 Dec;176:S297-396.

64. Cheung KG, Cole LK, Xiang B, Chen K, Ma X, Myal Y, et al. Sirtuin-3 (SIRT3) Protein Attenuates Doxorubicin-induced Oxidative Stress and Improves Mitochondrial Respiration in H9c2 Cardiomyocytes. Journal of Biological Chemistry. 2015 Apr 24;290(17):10981–93.

65. Koentges C, Pfeil K, Schnick T, Wiese S, Dahlbock R, Cimolai MC, Meyer-Steenbuck M, Cenkerova K, Hoffmann MM, Jaeger C, Odening KE. SIRT3 deficiency impairs mitochondrial and contractile function in the heart. Basic research in cardiology. 2015 Jul 1;110(4):36.

66. Ma S, Feng J, Zhang R, Chen J, Han D, Li X, et al. SIRT1 Activation by Resveratrol Alleviates Cardiac Dysfunction via Mitochondrial Regulation in Diabetic Cardiomyopathy Mice. Oxidative Medicine and Cellular Longevity. 2017;2017:1–15.

67. Chang H-C, Guarente L. SIRT1 and other sirtuins in Metabolism. Trends Endocrinol Metab. 2014 Mar;25(3):138–45.

68. Liu M-H, Shan J, Li J, Zhang Y, Lin X-L. Resveratrol inhibits doxorubicin-induced cardiotoxicity via sirtuin 1 activation in H9c2 cardiomyocytes. Experimental and Therapeutic Medicine. 2016 Aug;12(2):1113–8.

69. Lee Chi Fung, Chavez Juan D., Garcia-Menendez Lorena, Choi Yongseon, Roe Nathan D., Chiao Ying Ann, et al. Normalization of NAD+ Redox Balance as a Therapy for Heart Failure. Circulation. 2016 Sep 20;134(12):883–94.

70. Peserico A, Simone C. Physical and functional HAT/HDAC interplay regulates protein acetylation balance. Biomed Research International. 2011 Oct;2011.

71. Barneda-Zahonero B, Parra M. Histone deacetylases and cancer. Molecular Oncology. 2012 Dec 1;6(6):579–89.

72. Rahman MM, Kukita A, Kukita T, Shobuike T, Nakamura T, Kohashi O. Two histone deacetylase inhibitors, trichostatin A and sodium butyrate, suppress differentiation into osteoclasts but not into macrophages. Blood. 2003 May 1;101(9):3451–9.

73. Saha R, Pahan K. HATs and HDACs in neurodegeneration: a tale of disconcerted acetylation homeostasis. Cell Death Differ. 2006 Apr;13(4):539–50.

74. Zheng S, Koh XY, Goh HC, Rahmat SAB, Hwang L-A, Lane DP. Inhibiting p53 Acetylation Reduces Cancer Chemotoxicity. Cancer Res. 2017 Aug 15;77(16):4342–54.

75. Ma J, Wang Y, Zheng D, Wei M, Xu H, Peng T. Rac1 signalling mediates doxorubicin-induced cardiotoxicity through both reactive oxygen species-dependent and -independent pathways. Cardiovascular Research. 2013 Jan 1;97(1):77–87.

76. Karagiannis TC, Lin AJ, Ververis K, Chang L, Tang MM, Okabe J, et al. Trichostatin A accentuates doxorubicin-induced hypertrophy in cardiac myocytes. Aging. 2010 Sep 17;2(10):659–68.

77. Glozak MA, Sengupta N, Zhang X, Seto E. Acetylation and deacetylation of non-histone proteins. Gene. 2005 Dec 19;363:15–23.

78. Wang Y, Miao X, Liu Y, Li F, Liu Q, Sun J, et al. Dysregulation of Histone Acetyltransferases and Deacetylases in Cardiovascular Diseases. Oxidative Medicine and Cellular Longevity. 2014;2014:1–11.

79. Han Y, Jin Y-H, Kim Y-J, Kang B-Y, Choi H-J, Kim D-W, et al. Acetylation of Sirt2 by p300 attenuates its deacetylase activity. Biochemical and Biophysical Research Communications. 2008 Oct 31;375(4):576–80.

80. Barlev NA, Liu L, Chehab NH, Mansfield K, Harris KG, Halazonetis TD, et al. Acetylation of p53 Activates Transcription through Recruitment of Coactivators/Histone Acetyltransferases. Molecular Cell. 2001 Dec 1;8(6):1243–54.

81. Nagy Z, Tora L. Distinct GCN5/PCAF-containing complexes function as co-activators and are involved in transcription factor and global histone acetylation. Oncogene. 2007 Aug;26(37):5341–57.

82. Salah Ud-Din A, Tikhomirova A, Roujeinikova A. Structure and Functional Diversity of GCN5-Related N-Acetyltransferases (GNAT). International Journal of Molecular Sciences. 2016 Jun 28;17(7):1018.

83. Biel M, Kretsovali A, Karatzali E, Papamatheakis J, Giannis A. Design, synthesis, and biological evaluation of a small-molecule inhibitor of the histone acetyltransferase Gcn5. Angew Chem Int Ed Engl. 2004 Jul 26;43(30):3974–6.

84. Mai A, Rotili D, Tarantino D, Ornaghi P, Tosi F, Vicidomini C, et al. Small-Molecule Inhibitors of Histone Acetyltransferase Activity: Identification and Biological Properties. Journal of Medicinal Chemistry. 2006 Nov;49(23):6897–907.

85. Sapountzi V, Côté J. MYST-family histone acetyltransferases: beyond chromatin. Cell Mol Life Sci. 2011 Apr 1;68(7):1147–56.

86. Fisher JB, Horst A, Wan T, Kim M-S, Auchampach J, Lough J. Depletion of Tip60 from In Vivo Cardiomyocytes Increases Myocyte Density, Followed by Cardiac Dysfunction, Myocyte Fallout and Lethality. Xu X, editor. PLOS ONE. 2016 Oct 21;11(10):e0164855.

87. Chen D, Li N, Wang Y, Wu X, Wang B. A mini review about Tip60 functional mechanism: A potential therapeutic target in cardiovascular disease.

88. Stixova L, Strnad H, Kozubek S, Martinet N, Dekker FJ, Franek M, et al. Basic nuclear processes affected by histone acetyltransferases and histone deacetylase inhibitors. Epigenomics. 2013 Aug;5(4):379-.

89. Su J, Wang F, Cai Y, Jin J. The Functional Analysis of Histone Acetyltransferase MOF in Tumorigenesis. International Journal of Molecular Sciences. 2016 Jan;17(1):99.

90. Ghizzoni M, Wu J, Gao T, Haisma HJ, Dekker FJ, George Zheng Y. 6-alkylsalicylates are selective Tip60 inhibitors and target the acetyl-CoA binding site. European Journal of Medicinal Chemistry. 2012 Jan 1;47:337–44.

91. MG 149 (Tip60 HAT inhibitor) Histone Acetyltransferase Inhibitor | MedChemExpress. Available from: https://www.medchemexpress.com/mg-149.html

92. Trisciuoglio D, Di Martile M, Del Bufalo D. Emerging Role of Histone Acetyltransferase in Stem Cells and Cancer. Stem Cells International. 2018 Dec 16;2018:1–11.

93. Nakagawa Yasuaki, Kuwahara Koichiro, Takemura Genzo, Akao Masaharu, Kato Masashi, Arai Yuji, et al. p300 Plays a Critical Role in Maintaining Cardiac Mitochondrial Function and Cell Survival in Postnatal Hearts. Circulation Research. 2009 Oct 9;105(8):746–54.

94. Yanazume T, Morimoto T, Wada H, Kawamura T, Hasegawa K. Biological role of p300 in cardiac myocytes. Molecular and cellular biochemistry. 2003 Jun 1;248(1-2):115-9.

95. Pietrocola F, Lachkar S, Enot DP, Niso-Santano M, Bravo-San Pedro JM, Sica V, et al. Spermidine induces autophagy by inhibiting the acetyltransferase EP300. Cell Death & Differentiation. 2015 Mar;22(3):509–16.

96. Costi R, Di Santo R, Artico M, Miele G, Valentini P, Novellino E, et al. Cinnamoyl Compounds as Simple Molecules that Inhibit p300 Histone Acetyltransferase. Journal of Medicinal Chemistry. 2007 Apr;50(8):1973–7.

97. Bowers EM, Yan G, Mukherjee C, Orry A, Wang L, Holbert MA, et al. Virtual Ligand Screening of the p300/CBP Histone Acetyltransferase: Identification of a Selective Small Molecule Inhibitor. Chemistry & Biology. 2010 May;17(5):471–82.

98. Watkins SJ, Borthwick GM, Arthur HM. The H9C2 cell line and primary neonatal cardiomyocyte cells show similar hypertrophic responses in vitro. In Vitro Cellular & Developmental Biology - Animal. 2011 Feb;47(2):125–31.

99. Hanf A, Oelze M, Manea A, Li H, Münzel T, Daiber A. The anti-cancer drug doxorubicin induces substantial epigenetic changes in cultured cardiomyocytes. Chemico-Biological Interactions. 2019 Nov 1;313:108834.

100. Sardão VA, Oliveira PJ, Holy J, Oliveira CR, Wallace KB. Morphological alterations induced by doxorubicin on H9c2 myoblasts: nuclear, mitochondrial, and cytoskeletal targets. Cell Biol Toxicol. 2009 Jun 1;25(3):227–43.

101. Turakhia S, Venkatakrishnan CD, Dunsmore K, Wong H, Kuppusamy P, Zweier JL, et al. Doxorubicin-induced cardiotoxicity: direct correlation of cardiac fibroblast and H9c2 cell survival and aconitase activity with heat shock protein 27. American Journal of Physiology-Heart and Circulatory Physiology. 2007 Nov;293(5):H3111–21.

102. Witek P, Korga A, Burdan F, Ostrowska M, Nosowska B, Iwan M, et al. The effect of a number of H9C2 rat cardiomyocytes passage on repeatability of cytotoxicity study results. Cytotechnology. 2016 Dec;68(6):2407–15.

103. Liu L, Wang P, Liu X, He D, Liang C, Yu Y. Exogenous NAD+ supplementation protects H9c2 cardiac myoblasts against hypoxia/reoxygenation injury via Sirt1-p53 pathway. Fundamental & Clinical Pharmacology. 2014;28(2):180–9.

104. Luo G, Jian Z, Zhu Y, Zhu Y, Chen B, Ma R, Tang F, Xiao Y. Sirt1 promotes autophagy and inhibits apoptosis to protect cardiomyocytes from hypoxic stress. International journal of molecular medicine. 2019 May 1;43(5):2033-43.

105. Schipke J, Banmann E, Nikam S, Voswinckel R, Kohlstedt K, Loot AE, et al. The number of cardiac myocytes in the hypertrophic and hypotrophic left ventricle of the obese and calorie-restricted mouse heart. Journal of Anatomy. 2014 Nov;225(5):539–47.

106. Bensley JG, De Matteo R, Harding R, Black MJ. Three-dimensional direct measurement of cardiomyocyte volume, nuclearity, and ploidy in thick histological sections. Scientific reports. 2016 Apr 6;6(1):1-0.

107. Mills KF, Yoshida S, Stein LR, Grozio A, Kubota S, Sasaki Y, et al. Long-Term Administration of Nicotinamide Mononucleotide Mitigates Age-Associated Physiological Decline in Mice. Cell Metabolism. 2016 Dec;24(6):795–806.

108. Yoshino J, Mills KF, Yoon MJ, Imai S. Nicotinamide Mononucleotide, a Key NAD+ Intermediate, Treats the Pathophysiology of Diet- and Age-Induced Diabetes in Mice. Cell Metabolism. 2011 Oct;14(4):528–36.

109. Peng L, Qian M, Liu Z, Tang X, Sun J, Jiang Y, et al. Deacetylase-independent function of SIRT6 couples GATA4 transcription factor and epigenetic activation against cardiomyocyte apoptosis. Nucleic Acids Research. 2020 May 21;48(9):4992–5005.

110. Djouder N. New Insights About Doxorubicin-Induced Toxicity to Cardiomyoblast-Derived H9C2 Cells and Dexrazoxane Cytoprotective Effect: Contribution of In Vitro 1H-NMR Metabonomics. Molecular & Cellular Oncology. 2015 Oct 2;2(4):e1001199.

111. Demarest TG, Babbar M, Okur MN, Dan X, Croteau DL, Fakouri NB, et al. NAD+ Metabolism in Aging and Cancer. 2019;28.

112. McCullough SD, Grant PA. Histone acetylation, acetyltransferases, and ataxia—alteration of histone acetylation and chromatin dynamics is implicated in the pathogenesis of polyglutamine-expansion disorders. InAdvances in protein chemistry and structural biology 2010 Jan 1 (Vol. 79, pp. 165-203). Academic Press.

113. Tummala KS, Gomes AL, Yilmaz M, Graña O, Bakiri L, Ruppen I, et al. Inhibition of De Novo NAD + Synthesis by Oncogenic URI Causes Liver Tumorigenesis through DNA Damage. Cancer Cell. 2014 Dec;26(6):826–39.

114. Gajer JM, Furdas SD, Gründer A, Gothwal M, Heinicke U, Keller K, et al. Histone acetyltransferase inhibitors block neuroblastoma cell growth in vivo. Oncogenesis. 2015 Feb;4(2):e137–e137.

Curriculum Vitae

Name:	Rebecca Dang
Post-secondary Education and Degrees:	The University of Western Ontario London, Ontario, Canada 2018-2020 M.Sc McMaster University Hamilton, Ontario, Canada 2013-2018 B.Sc
Honours and Awards:	Gradate Research Scholarship The University of Western Ontario 2018-2020 Honours Entrance Scholarship McMaster University 2013
Related Work Experience	Biology 1101/1201 Teaching Assistant The University of Western Ontario 2019

Poster Presentations:

Dang, R., Ni, R., & Peng, T. *Increased acetylation of Vacuolar H^+ ATPase V0 D1 subunit during Doxorubicin-induced cardiotoxicity*. Poster Presentation at Western University's Pathology & Laboratory Research Day, March 2019. London, ON.

Dang, R., Ni, R., & Peng, T. *Increased acetylation of Vacuolar H^+ ATPase V0 D1 subunit during Doxorubicin-induced cardiotoxicity*. Poster Presentation at Western Research Forum, March 2019. London, ON.